JOURNAL OF RESEARCH of the National Bureau of Standards—C. Engineering and Instrumentation
Vol. 65C, No. 4, October–December 1961

Radiation Field From a Circular Disk Source[1]

J. H. Hubbell, R. L. Bach, and R. J. Herbold

(February 4, 1961)

A number of radiation shielding problems involve calculations of the response of an isotropic detector to radiation of arbitrary angular distribution from uniform finite plane sources. Series expansion methods previously used for treating the rectangular source are here extended to include the circular disk source with detector off-axis. These methods involve the family of integrals $\int_S (\cos\theta\, dS/r^2) P_l(\cos\theta)$ and the integral $\int_S (dS/r^2) \exp(-\mu r)$ where θ is obliquity with respect to the normal to the disk surface S, r is the distance from an element of source area, dS, to the detector, and μ is the attenuation coefficient. Tabulations of the first type of integral facilitate use of Legendre expansion representations of radiation directional distributions. The second integral relates primarily to exponentially attenuated radiation from a plane isotropic disk source, but the expansion coefficient solution can be readily adapted to take into account a point isotropic buildup factor of the polynomial form $\sum_{i=0}^{N} \beta_i(\mu r)^i$. This adaptation applies equally well to the corresponding expansion coefficients previously given for the rectangular source. Formulas and numerical results are presented.

1. Introduction

In radiation shielding, photometry and related studies, a frequently occurring problem is that of calculating the radiation field resulting from a finite plane source of radiation with arbitrary polar angular distribution $g(\theta)$. A number of authors have investigated the response of surface-type [1][2] detectors to rectangular and circular Lambert's-law radiators. Smith and Storm [2] have derived a generalized series expansion method for calculating the response of an azimuthally symmetric detector off-axis from a disk source with arbitrary surface angular distribution, in which evaluation of the series terms involves successive differentiation of the detector response to a differential element of the source area. The resulting formulas usually consist of triple or quadruple summations in which one sum can be obtained by recursion methods.

In a previous paper [3], a Legendre expansion method suggested by Berger and Lamkin [4] was applied to a rectangular source as part of a general study of the penetration of radiation into structures [5]. In the Berger-Lamkin method, the *geometric* relationship of detector to source is characterized by a set of Legendre coefficients, p_l, over which corresponding *penetration*-dependent coefficients, g_l, of a Legendre expansion of $g(\theta)$ may be summed. This has some advantage over the results in reference [2] in that not only are the geometrical and penetration parameters separated for economy of data tabulation, but use of the present Spencer-Fano [6] moments method provides most directly the g_l coefficients, rather than the actual angular distributions $g(\theta)$.

For small values of μt, where μ is the attenuation coefficient and t is the barrier thickness, the Legendre series solution does not converge adequately for the particular angular distribution for the unscattered radiation from a plane isotropic source [3]

$$g(\theta) = g^o(\theta) \equiv (\sigma/4\pi) \exp(-\mu t/\cos\theta)/\cos\theta, \quad (1)$$

in which $\sigma/4\pi$ is the source strength in units of radiation (e.g., photons) emitted per unit time from unit surface area into unit solid angle. The reason for this poor convergence is that, as $\mu t \to 0$, $g^o(\theta) \to (\sigma/4\pi)/\cos\theta$, and a function of the form $1/\cos\theta$ is not representable by the *positive* powers of $\cos\theta$ appearing in the Legendre polynomials. An alternative series expansion in powers of μt with geometry dependent coefficients, q_n, was provided for calculating the unscattered radiation component when $0 \leq \mu t \lesssim 1$.

The present work extends the two expansion methods in reference [3] to include the case of a circular disk source with detector off-axis. A typical example of this situation would be the estimation of the neutron flux around the face of a cylindrical thermal column of a research reactor [7]. In addition, it will be shown that if the scattering properties of the medium are given as a point isotropic buildup factor [6] in polynomial form [8, 9]

$$B(\mu r) \cong \sum_{i=0}^{N} \beta_i(\mu r)^i, \quad (2)$$

rather than as angular harmonics, g_l, at the exit surface of the barrier, the q_n expansion coefficients here and in reference [3] can often be used to evaluate the scattered as well as unscattered contribution to the radiation flux.

[1] Work supported jointly by the Office of Civil and Defense Mobilization the Navy Bureau of Yards and Docks, and the Defense Atomic Support Agency
[2] Figures in brackets indicate the literature references at the end of this paper.

[3] Here and in what follows, g^o and I^o will be used to denote the angular distribution and intensity of direct radiation, i.e., radiation which arrives at the detector from the source after having undergone no scattering interactions with the intervening medium.

2. Arbitrary Angular Distribution; Legendre Expansion of the Angular Response Function

2.1. Isotropic Detector (Flux)

If the emission from each source element, dS, of the disk, is independent of azimuth and uniform over the source surface S, the radiation intensity at any point in space, as measured by a small spherically symmetric detector, may be written as the integral

$$I=\int g(\theta)\cdot\psi_S(\theta)d(\cos\theta). \tag{3}$$

Here θ is the polar angle as indicated in figure 1. The angular distribution function $g(\theta)$ of radiation crossing the source-plane will now be defined as the radiation flux [4] (e.g., photons) traveling in direction θ per unit solid angle, unit time, and unit area normal to direction θ. $\psi_S(\theta)$, called the "angular response function" in reference [4], is the azimuthal angle subtended by the source area from the detector-to-source-plane vertical for a given θ-cone around this vertical.

There are a variety of ways in which the integral (3) may be evaluated, depending on the nature of $g(\theta)$ and S. The Legendre expansion method, especially advantageous if g_l coefficients happen to be already available, has been discussed in detail in references [3] and [4], but for convenience a brief summary is given as follows:

The two functions, $g(\theta)$ and $\psi_S(\theta)$, in (3) which are parametrically independent except in θ, may (if free of singularities) be expanded in Legendre harmonics as

$$g(\theta)=\sum_{l=0}^{\infty}(l+\tfrac{1}{2})g_l\cdot P_l(\cos\theta) \tag{4}$$

and

$$\psi_S(\theta)=\sum_{l=0}^{\infty}(l+\tfrac{1}{2})p_l\cdot P_l(\cos\theta). \tag{5}$$

[4] In this notation the radiation flux in direction θ per unit solid angle, unit time and *unit area of the source* would be $g(\theta)\cos\theta$, i.e., $g(\theta)$ may be identified with the angular distribution functions $g(z,\theta)$ and $\phi(\mu)$ of references [4] and [7], respectively, but differs from $G(R)$ of reference [2] according to $g(\theta)=G(R)/\cos\theta$.

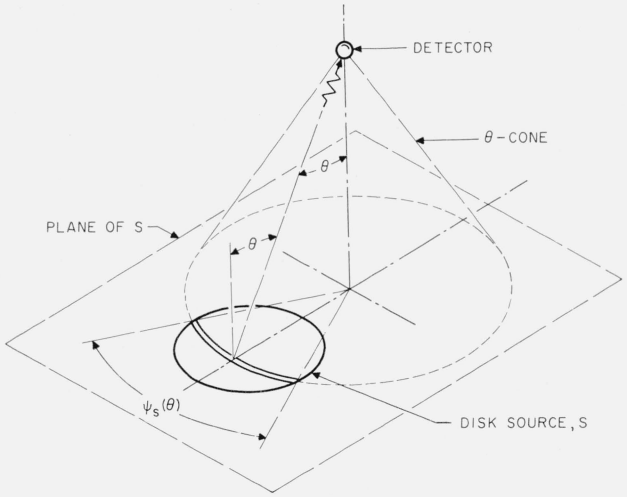

FIGURE 1. *Disk source and off-axis detector, showing polar angle θ and "angular response function," $\psi_S(\theta)$.*

When this is done, the integral (3) may be written as the series

$$I=\sum_{l=0}^{\infty}(l+\tfrac{1}{2})g_l\cdot p_l \tag{6}$$

which converges rapidly for many cases of interest.

The p_l coefficients may be evaluated in the usual way according to

$$p_l=\int_S P_l(\cos\theta)\cdot\psi_S(\theta)d(\cos\theta), \tag{7}$$

or since $\psi_S(\theta)d(\cos\theta)$ is a differential solid angle $d\Omega_S(\theta)$,

$$p_l=\int_S P_l(\cos\theta)d\Omega_S(\theta) \tag{8}$$

As in reference [3], the $\psi_S(\theta)$ and related p_l's are dependent on the relative, rather than on the absolute dimensions, so that we may select one dimension, here the disk radius, as the unit of length. The quantities ρ and h, as indicated in figure 2, are then the distances off axis and off disk-plane, respectively, measured in disk radii.

Since the polynomials $P_l(\cos\theta)$ are linear combinations of even or odd powers of $(\cos\theta)$ it is convenient to break up (8) into components $F_j(\rho,h)$, each over a particular power of $\cos\theta$, i.e.

$$F_j(\rho,h)=\int_S\cos^j\theta d\Omega(\theta,\rho,h), \tag{9}$$

from which we reconstruct the desired functions $p_l(\rho,h)$ according to

$$p_l(\rho,h)=\sum a_{lj}F_j(\rho,h), \tag{10}$$

where a_{lj} are the coefficients of x^j in the Legendre polynomial

$$P_l(x)=\sum a_{lj}x^j$$

of order l.

The differential solid angle, $d\Omega(\theta,\rho,h)$, can be written in cylindrical coordinates h, R, and ϕ around

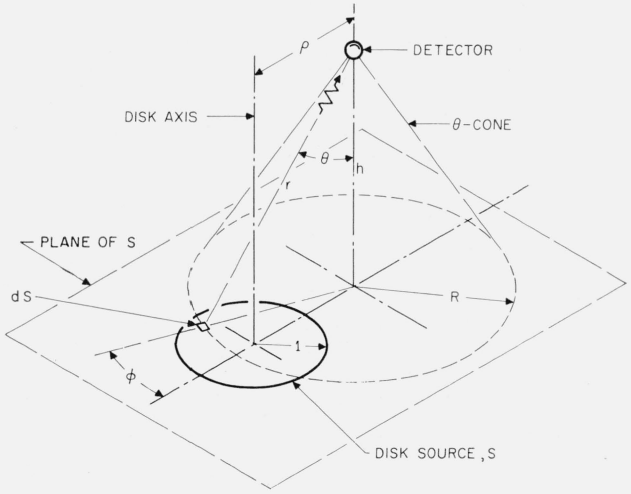

FIGURE 2. *Source-detector geometry, showing relevant parameters ρ, h, θ, ϕ, r and R, in which linear dimensions are measured in radii of the source disk.*

the perpendicular from detector to source-plane as

$$d\Omega(\theta,\rho,h)=\cos\theta\, dS/r^2=(h^2+R^2)^{-3/2}hR\, dR\, d\phi, \quad (11)$$

since $\cos\theta=h/\sqrt{h^2+R^2}$, $dS=R\, dR\, d\phi$, and $r^2=h^2+R^2$. The integral in (9) may now be written explicitly as the double integral [5]

$$F_j(\rho,h) = h^{j+1}\int_{R=\rho-1}^{\rho+1}\int_{\phi=-1/2\psi(\theta,\rho,h)}^{1/2\psi(\theta,\rho,h)}(h^2+R^2)^{-(j+3)/2}R\, d\, Rd\phi, \quad (12)$$

in which the limits $\pm\frac{1}{2}\psi(\theta,\rho,h)$ of the azimuthal variable ϕ are indicated in figures 1 and 2. The angular response function $\psi(\theta,\rho,h)$ is the quantity $\psi_S(\theta)$ defined following eq (3), in which the generalized source-detector geometry symbol S has been replaced by the parameters ρ and h which characterize the disk source situation.

Now, since

$$\psi(\theta,\rho,h)=2\cos^{-1}\{(\rho^2+R^2-1)/2\rho R\}, \quad (13)$$

we may write (12) as the single integral

$$F_j(\rho,h)=h^{j+1}\int_{R=\rho-1}^{\rho+1}2R\, dR(h^2+R^2)^{-(j+3)/2} \times\cos^{-1}\{(\rho^2+R^2-1)/2\rho R\}. \quad (14)$$

Integration by parts and use of the substitution

$$R^2=\rho^2+1-2\rho\cos t \quad (15)$$

transforms (14) to the form

$$F_j(\rho,h)=\frac{h^{j+1}}{j+1}\times \left\{(\rho^2-1)\int_0^\pi \frac{dt}{(\rho^2+1-2\rho\cos t)(h^2+\rho^2+1-2\rho\cos t)^{\frac{j+1}{2}}} -\int_0^\pi \frac{dt}{(h^2+\rho^2+1-2\rho\cos t)^{\frac{j+1}{2}}}\right\}. \quad (16)$$

The first of the two integrals in (16) may be further reduced by use of the identity

$$\frac{1}{a^2(h^2+a^2)^j}=\frac{1}{a^2h^{2j}}-\sum_{i=0}^{j-1}\frac{1}{h^{2j-2i}}\cdot\frac{1}{(h^2+a^2)^{i+1}}, \quad (17)$$

in which $a^2=\rho^2+1-2\rho\cos t$.

Since at this point the evaluation of the integral for the case of odd j (and thus odd l) is quite different from that for even j, these cases will be treated separately in subsections A and B, as follows:

[5] The limits of integration $\rho-1$, $\rho+1$ in (12) refer to the case $1\leq\rho\leq\infty$. For $0\leq\rho<1$ the integral should be split into the ranges $0\leq R\leq 1-\rho$ and $1-\rho\leq R\leq 1+\rho$. However, the resulting expressions are identical.

A. Even j,l

Combining (16) and (17) we have for the F-integrals for even j, denoted as F_{2j}, where $j=0$, 1, 2 . . .,

$$F_{2j}(\rho,h)=\frac{h^{2j+1}}{2j+1} \times\left\{\frac{\rho^2-1}{h^{2j}}\int_0^\pi\frac{dt}{(\rho^2+1-2\rho\cos t)\sqrt{h^2+\rho^2+1-2\rho\cos t}} -(\rho^2-1)\left[\sum_{i=0}^{j-1}\frac{1}{h^{2j-2i}}\int_0^\pi\frac{dt}{(h^2+\rho^2+1-2\rho\cos t)^{i+3/2}}\right] -\int_0^\pi\frac{dt}{(h^2+\rho^2+1-2\rho\cos t)^{j+1/2}}\right\}. \quad (18)$$

The first integral in (18) can be evaluated in terms of complete and incomplete elliptic integrals of the first and second kinds. However, in combining these F_{2j}'s according to (10) to give p_{2l}, it can be shown that for $l>0$ this integral cancels out, i.e., the polynomial $\sum a_{lj}(2j+1)^{-1}$ has the properties

$$\sum a_{lj}(2j+1)^{-1}=\begin{bmatrix}1 \text{ for } l=0\\ 0 \text{ for } l>0, l \text{ even}\end{bmatrix}. \quad (19)$$

The zeroth coefficient $p_0(\rho,h)$ (which is the same as $F_0(\rho,h)$) is the response of an isotropic detector, at an off-axis position ρ,h, to radiation from a "perfectly diffuse" circular disk source, i.e., $g(\theta)=$ constant. Fortunately, $p_0(\rho,h)$ is also the solid angle subtended by a circular disk from the point ρ,h, and in the latter role has been discussed and evaluated by a number of authors [10, 11]. If we use one of these tabulations [6] for p_0, we need only evaluate the integral appearing in (18) in the summation and also in the final term. Factoring out the quantity $(h^2+\rho^2+1)^{-(n+1/2)}$ from this integral reduces it to the form

$$S_n(k)=\int_0^\pi(1-k^2\cos t)^{-(n+1/2)}dt, \quad (20)$$

in which n corresponds to the i and j in (18) and $k^2=2\rho/(h^2+\rho^2+1)\leq 1$. This family of integrals may be evaluated in terms of complete elliptic integrals of the first and second kinds [12].

$$S_0(k)=\frac{2}{\sqrt{1+k^2}}K\left(\sqrt{\frac{2k^2}{1+k^2}}\right), \quad (21)$$

$$S_1(k)=\frac{2}{(1-k^2)\sqrt{1+k^2}}E\left(\sqrt{\frac{2k^2}{1+k^2}}\right), \quad (22)$$

and for $n\geq 2$,

$$S_n(k)=\frac{1}{1-k^4}\left\{\left(1+\frac{2n-3}{2n-1}\right)S_{n-1}-\frac{2n-3}{2n-1}S_{n-2}\right\}. \quad (23)$$

[6] For tabulations of p_0 see, for example, references [10] and [11]. The parameters ρ and h in this paper were explicitly selected in order to use directly the extensive table in reference [11].

Extensive tabulations [13] of K and E exist in addition to an excellent polynomial approximation by Hastings [14] suitable for use on a high-speed computer.

Substituting (20) into (18) we have

$$F_{2j}(\rho,h)=\{\text{cancellation terms in } p_{2l}(\rho,h) \text{ for } l>0\}$$
$$-\frac{1}{2j+1}\left\{\left(\frac{h^2}{h^2+\rho^2+1}\right)^{j+1/2}S_j(k)+\frac{\rho^2-1}{h^2}\sum_{i=1}^{j}\left(\frac{h^2}{h^2+\rho^2+1}\right)^{i+1/2}S_i(k)\right\}. \quad (24)$$

The even-l response function coefficients $p_{2l}(\rho,h)$ may then be built up from the $F_{2j}(\rho,h)$'s in (24) as indicated in (10). Equation (10) may be written more explicitly for even l as

$$p_{2l}(\rho,h)=\sum_{j=0}^{l}\frac{(-1)^j}{2^{2l}}\binom{2l-j}{j}\binom{4l-2j}{2l-j}F_{2l-2j}(\rho,h), \quad (25)$$

in which the quantity

$$\binom{n}{r}=\frac{n!}{r!(n-r)!} \quad (26)$$

is the rth coefficient of an nth degree binomial expansion.

B. Odd j,l

Denoting the odd-j F-integrals in (16) as $F_{2j+1}(\rho,h)$ where $j=0, 1, 2, \ldots$, we have, using (17),

$$F_{2j+1}(\rho,h)=\frac{1}{2j+2}\left\{(\rho^2-1)\int_0^{\pi}\frac{dt}{(\rho^2+1-2\rho\cos t)}-\frac{\rho^2-1}{h^2}\left[\sum_{i=0}^{j}h^{2i+2}\int_0^{\pi}\frac{dt}{(h^2+\rho^2+1-2\rho\cos t)^{i+1}}\right]-h^{2j+2}\int_0^{\pi}\frac{dt}{(h^2+\rho^2+1-2\rho\cos t)^{j+1}}\right\}. \quad (27)$$

Since the integrand denominators have integers, rather than half-integers, as exponents, closed-form algebraic expressions result, rather than quantities in terms of tabulated higher functions or infinite series expansions. Use of standard integral tables [15] to evaluate (27) gives

$$F_{2j+1}(\rho,h)=\frac{\pi}{2j+2}\left\{1-\left(\frac{h^2}{\sqrt{(h^2-\rho^2+1)^2+4\rho^2h^2}}\right)^{j+1}P_j\left(\frac{h^2+\rho^2+1}{\sqrt{(h^2-\rho^2+1)^2+4\rho^2h^2}}\right)-\frac{\rho^2-1}{h^2}\sum_{i=0}^{j}\left(\frac{h^2}{\sqrt{(h^2-\rho^2+1)^2+4\rho^2h^2}}\right)^{i+1}\times P_i\left(\frac{h^2+\rho^2+1}{\sqrt{(h^2-\rho^2+1)^2+4\rho^2h^2}}\right)\right\}, \quad (28)$$

in which $(\cos\theta)^m$ is replaced by

$$\{(h^2+\rho^2+1)/\sqrt{(h^2-\rho^2+1)^2+4\rho^2h^2}\}^m$$

in the usual Legendre polynomials $P_n(\cos\theta)$ to give the quantities P_i and P_j in (28).

Substituting (28) into (10), we have for the first two odd-l coefficients

$$p_1(\rho,h)=\frac{\pi}{2}\left(1-\frac{h^2+\rho^2-1}{\sqrt{(h^2-\rho^2+1)^2+4\rho^2h^2}}\right) \quad (29)$$

and

$$p_3(\rho,h)=\frac{\pi}{8}\left\{-1+\frac{6h^2+\rho^2-1}{\sqrt{(h^2-\rho^2+1)^2+4\rho^2h^2}}-\frac{5h^2(h^2+\rho^2-1)(h^2+\rho^2+1)}{[(h^2-\rho^2+1)^2+4\rho^2h^2]^{3/2}}\right\}. \quad (30)$$

The higher odd-l terms can be written in a form comparable to (25) as

$$p_{2l+1}(\rho,h)=\sum_{j=0}^{l}\frac{(-1)^j}{2^{2l+1}}\times\binom{2l-j+1}{j}\binom{4l-2j+2}{2l-j+1}F_{2l-2j+1}(\rho,h) \quad (31)$$

using the $F_{2j+1}(\rho,h)$'s from (28).

The $p_1(\rho,h)$ coefficient in (29) is equivalent to the response of a plane detector parallel to the plane of a perfectly diffuse (Lambert's law) uniform circular disk source, and has been derived and discussed by a number of authors [16].

The $F_{2j}(\rho,h)$ and $F_{2j+1}(\rho,h)$ expressions in (24) and (28), and the expressions in (25) and (31) for their respective Legendre combinations were programed for evaluation of the $p_l(\rho,h)$'s on an IBM 704 computer. The resulting numerical values for the $p_l(\rho,h)$ are presented in table 1 for $0\leq\rho\leq10$, $0.1\leq h\leq10$ and $1\leq l\leq13$. The entries for $p_0(\rho,h)$ were taken from reference [11]. For ρ or h greater than 10, the source may be treated for all practical purposes as a point anisotropic source with the same angular distribution, $g(\theta)\cos\emptyset$, as each surface element of the source. The $p_l(\rho,h)$ coefficients in table 1 may now be combined with g_l coefficients as in equation (6) to give the radiation flux intercepted by a small spherical detector at coordinates ρ,h.

As a check on these $p_l(\rho,h)$'s, they may be inserted in (5) to reconstruct the angular response function $\psi(\theta,\rho,h)$. Three detector positions ($\rho=0.5$, $h=0.5$; $\rho=1$, $h=1$; $\rho=2$, $h=1$) are indicated in figure 3, and the exact angular response functions for these positions are given by the solid lines in figure 4. Summing over the first 10 terms in (5) gives us the approximations shown by the dashed lines in figure 4.

2.2. Cosine Detector

As has been discussed in reference [3], a similar analysis of a finite uniform plane source geometry may be performed in the case of a surface-element detector with response proportional to the cosine of the angle of incidence of the radiation. For the case of a surface-element detector parallel to the

TABLE 1.* *Coefficients $p_l(\rho,h)$ of the Legendre expansion (5) of the angular response function $\psi(\theta,\rho,h)$*

$p_l(\rho, h)$

h	l \ ρ	0	0.2	0.5	0.8	1.0
0.1	0	5.6580 (0)	5.6389 (0)	5.5092 (0)	4.9511 (0)	2.7036 (0)
	1	3.1105 (0)	3.1079 (0)	3.0872 (0)	2.9346 (0)	1.4924 (0)
	2	3.0951 (−1)	3.1855 (−1)	3.7857 (−1)	5.9042 (−1)	1.6880 (−1)
	3	−7.3913 (−1)	−7.3534 (−1)	−7.0554 (−1)	−5.1185 (−1)	−3.2419 (−1)
	4	−2.2677 (−1)	−2.3270 (−1)	−2.6957 (−1)	−3.3127 (−1)	−9.7153 (−2)
	5	3.3572 (−1)	3.3122 (−1)	2.9669 (−1)	1.2095 (−1)	1.4395 (−1)
	6	1.8207 (−1)	1.8596 (−1)	2.0681 (−1)	1.7067 (−1)	6.9956 (−2)
	7	−1.8038 (−1)	−1.7550 (−1)	−1.3959 (−1)	−1.8423 (−2)	−7.7337 (−2)
	8	−1.5130 (−1)	−1.5352 (−1)	−1.6127 (−1)	−7.5020 (−2)	−5.2967 (−2)
	9	1.0068 (−1)	9.5697 (−2)	6.1222 (−2)	5.8812 (−3)	4.6161 (−2)
	10	1.2734 (−1)	1.2811 (−1)	1.2488 (−1)	3.1191 (−2)	4.2324 (−2)
	11	−5.3333 (−2)	−4.8521 (−2)	−1.7867 (−2)	−1.7343 (−2)	−2.8446 (−2)
	12	−1.0734 (−1)	−1.0684 (−1)	−9.4741 (−2)	−2.2105 (−2)	−3.4397 (−2)
	13	2.2831 (−2)	1.8417 (−2)	−6.5421 (−3)	2.4535 (−2)	1.7852 (−2)
	l \ ρ	1.2	1.5	2.0	5.0	10.0
	0	6.0618 (−1)	1.7518 (−1)	5.3816 (−2)	2.6296 (−3)	3.1768 (−4)
	1	1.3539 (−1)	1.9422 (−2)	3.4561 (−3)	5.4493 (−5)	3.2047 (−6)
	2	−2.4825 (−1)	−8.3956 (−2)	−2.6553 (−2)	−1.3131 (−3)	−1.5879 (−4)
	3	−1.7525 (−1)	−2.8306 (−2)	−5.1412 (−3)	−8.1680 (−5)	−4.8063 (−6)
	4	1.0623 (−1)	5.6815 (−2)	1.9299 (−2)	9.8181 (−4)	1.1901 (−4)
	5	1.6643 (−1)	3.3581 (−2)	6.3309 (−3)	1.0196 (−4)	6.0060 (−6)
	6	−1.4981 (−2)	−3.9768 (−2)	−1.5289 (−2)	−8.1427 (−4)	−9.9063 (−5)
	7	−1.2740 (−1)	−3.6289 (−2)	−7.2270 (−3)	−1.1873 (−4)	−7.0039 (−6)
	8	−3.5553 (−2)	2.6539 (−2)	1.2454 (−2)	7.0782 (−4)	8.6547 (−5)
	9	7.8309 (−2)	3.6858 (−2)	7.9006 (−3)	1.3324 (−4)	7.8748 (−6)
	10	5.1249 (−2)	−1.5553 (−2)	−1.0188 (−2)	−6.3174 (−4)	−7.7741 (−5)
	11	−3.6546 (−2)	−3.5609 (−2)	−8.3855 (−3)	−1.4611 (−4)	−8.6560 (−6)
	12	−4.3885 (−2)	6.3576 (−3)	8.2513 (−3)	5.7324 (−4)	7.1095 (−5)
	13	1.1524 (−2)	3.2871 (−2)	8.7016 (−3)	1.5770 (−4)	9.3693 (−6)
0.2	l \ ρ	0	0.2	0.5	0.8	1.0
	0	5.0510 (0)	5.0156 (0)	4.7828 (0)	3.9593 (0)	2.4052 (0)
	1	3.0208 (0)	3.0113 (0)	2.9394 (0)	2.5521 (0)	1.4145 (0)
	2	5.9242 (−1)	6.0653 (−1)	6.9042 (−1)	8.1628 (−1)	2.6714 (−1)
	3	−6.0996 (−1)	−5.9725 (−1)	−5.0554 (−1)	−1.7057 (−1)	−2.5690 (−1)
	4	−4.0444 (−1)	−4.0939 (−1)	−4.2399 (−1)	−2.4971 (−1)	−1.4043 (−1)
	5	1.8601 (−1)	1.7310 (−1)	9.0334 (−2)	−7.4080 (−3)	9.3690 (−2)
	6	2.8843 (−1)	2.8648 (−1)	2.5294 (−1)	5.7523 (−2)	9.3989 (−2)
	7	−2.4333 (−2)	−1.3696 (−2)	4.0103 (−2)	−3.7853 (−2)	−3.5202 (−2)
	8	−2.0024 (−1)	−1.9326 (−1)	−1.3335 (−1)	−5.9687 (−2)	−6.4854 (−2)
	9	−4.9727 (−2)	−5.6315 (−2)	−7.1927 (−2)	2.6729 (−2)	1.0905 (−2)
	10	1.2879 (−1)	1.1895 (−1)	5.5438 (−2)	7.2910 (−2)	4.6952 (−2)
	11	8.1495 (−2)	8.3167 (−2)	6.2859 (−2)	1.8096 (−2)	1.7315 (−3)
	12	−7.0789 (−2)	−6.0437 (−2)	−1.2489 (−2)	−4.1686 (−2)	−3.3718 (−2)
	13	−8.8823 (−2)	−8.5486 (−2)	−4.0990 (−2)	−2.8918 (−2)	−7.7467 (−3)
	l \ ρ	1.2	1.5	2.0	5.0	10.0
	0	9.7005 (−1)	3.3005 (−1)	1.0554 (−1)	5.2489 (−3)	6.3507 (−4)
	1	3.6408 (−1)	7.0472 (−2)	1.3424 (−2)	2.1740 (−4)	1.2811 (−5)
	2	−2.4386 (−1)	−1.3978 (−1)	−5.0043 (−2)	−2.6108 (−3)	−3.1715 (−4)
	3	−3.4860 (−1)	−9.4767 (−2)	−1.9485 (−2)	−3.2513 (−4)	−1.9203 (−5)
	4	−5.6872 (−2)	6.5955 (−2)	3.2928 (−2)	1.9343 (−3)	2.3718 (−4)
	5	1.7291 (−1)	9.6607 (−2)	2.2940 (−2)	4.0426 (−4)	2.3975 (−5)
	6	1.2253 (−1)	−1.5020 (−2)	−2.1798 (−2)	−1.5809 (−3)	−1.9676 (−4)
	7	−3.1183 (−2)	−8.2335 (−2)	−2.4499 (−2)	−4.6802 (−4)	−2.7921 (−5)
	8	−6.7218 (−2)	−1.9212 (−2)	1.2973 (−2)	1.3466 (−3)	1.7111 (−4)
	9	−2.8126 (−3)	5.8673 (−2)	2.4463 (−2)	5.2123 (−4)	3.1338 (−5)
	10	2.3823 (−2)	3.7369 (−2)	−5.5921 (−3)	−1.1705 (−3)	−1.5279 (−4)
	11	−1.2139 (−2)	−3.2733 (−2)	−2.3072 (−2)	−5.6621 (−4)	−3.4373 (−5)
	12	−2.6654 (−2)	−4.1470 (−2)	−5.4447 (−4)	1.0276 (−3)	1.3873 (−4)
	13	9.2864 (−3)	1.0522 (−2)	2.0585 (−2)	6.0426 (−4)	3.7109 (−5)
0.5	l \ ρ	0	0.2	0.5	0.8	1.0
	0	3.4733 (0)	3.4184 (0)	3.1022 (0)	2.4123 (0)	1.7687 (0)
	1	2.5133 (0)	2.4802 (0)	2.2733 (0)	1.7426 (0)	1.1898 (0)
	2	1.1240 (0)	1.1232 (0)	1.0865 (0)	8.2414 (−1)	4.2719 (−1)
	3	0.0000	2.3936 (−2)	1.3416 (−1)	1.5252 (−1)	−7.3353 (−2)
	4	−4.4959 (−1)	−4.2364 (−1)	−2.6953 (−1)	−6.8444 (−2)	−1.6341 (−1)
	5	−3.0159 (−1)	−2.9631 (−1)	−2.1987 (−1)	6.2302 (−3)	−2.6599 (−2)
	6	4.4959 (−2)	2.5241 (−2)	−2.9195 (−2)	9.8306 (−2)	7.5291 (−2)
	7	2.2117 (−1)	1.9522 (−1)	6.6073 (−2)	7.1346 (−2)	4.7875 (−2)
	8	1.3488 (−1)	1.2808 (−1)	3.9757 (−2)	−1.6869 (−2)	−2.4193 (−2)
	9	−5.2276 (−2)	−3.2603 (−2)	−8.3723 (−3)	−5.7460 (−2)	−3.9902 (−2)
	10	−1.3847 (−1)	−1.1162 (−1)	−8.4522 (−3)	−2.8599 (−2)	−1.1920 (−4)
	11	−6.9165 (−2)	−6.2655 (−2)	1.9010 (−2)	8.6621 (−3)	2.8202 (−2)
	12	5.1793 (−2)	3.0551 (−2)	2.1923 (−2)	5.9185 (−3)	1.2729 (−2)
	13	9.5706 (−2)	6.8208 (−2)	−7.9961 (−3)	−2.0240 (−2)	−1.4838 (−2)

TABLE 1.* *Coefficients $p_l(\rho,h)$ of the Legendre expansion (5) of the angular response function ψ (θ,ρ,h)*—Continued

$p_l(\rho, h)$

h=0.5 l \ ρ	1.2	1.5	2.0	5.0	10.0
0	1.1661 (0)	5.9692 (−1)	2.3242 (−1)	1.2945 (−2)	1.5826 (−3)
1	6.7870 (−1)	2.6382 (−1)	6.9462 (−2)	1.3339 (−3)	7.9725 (−5)
2	6.7922 (−2)	−1.0857 (−1)	−8.3311 (−2)	−6.2644 (−3)	−7.8526 (−4)
3	−2.7369 (−1)	−2.3352 (−1)	−8.6034 (−2)	−1.9643 (−3)	−1.1908 (−4)
4	−2.4935 (−1)	−9.7788 (−2)	1.5867 (−2)	4.3407 (−3)	5.7842 (−4)
5	−6.2514 (−2)	8.1473 (−2)	7.3710 (−2)	2.3747 (−3)	1.4771 (−4)
6	4.6779 (−2)	1.1907 (−1)	2.6715 (−2)	−3.1647 (−3)	−4.6834 (−4)
7	2.2690 (−2)	3.0262 (−2)	−4.4313 (−2)	−2.6379 (−3)	−1.7041 (−4)
8	−3.1217 (−2)	−4.9324 (−2)	−4.5078 (−2)	2.2555 (−3)	3.9367 (−4)
9	−2.5263 (−2)	−4.4582 (−2)	1.1501 (−2)	2.7791 (−3)	1.8892 (−4)
10	2.1162 (−2)	9.5174 (−4)	4.2228 (−2)	−1.4823 (−3)	−3.3618 (−4)
11	4.0843 (−2)	1.7678 (−2)	1.3162 (−2)	−2.8121 (−3)	−2.0405 (−4)
12	1.7192 (−2)	6.0957 (−4)	−2.6483 (−2)	8.0073 (−4)	2.8842 (−4)
13	−8.5251 (−3)	−9.0943 (−3)	−2.4048 (−2)	2.7473 (−3)	2.1626 (−4)

h=1.0 l \ ρ	0	0.2	0.5	0.8	1.0
0	1.8403 (0)	1.8071 (0)	1.6371 (0)	1.3488 (0)	1.1227 (0)
1	1.5708 (0)	1.5394 (0)	1.3760 (0)	1.0921 (0)	8.6832 (−1)
2	1.1107 (0)	1.0855 (0)	9.4773 (−1)	6.9040 (−1)	4.8242 (−1)
3	5.8905 (−1)	5.7669 (−1)	4.9529 (−1)	3.0375 (−1)	1.3416 (−1)
4	1.3884 (−1)	1.4450 (−1)	1.4522 (−1)	5.4083 (−2)	−5.9580 (−2)
5	−1.4726 (−1)	−1.2475 (−1)	−4.2344 (−2)	−2.8548 (−2)	−8.8156 (−2)
6	−2.4297 (−1)	−2.1313 (−1)	−8.4731 (−2)	5.7923 (−4)	−2.6783 (−2)
7	−1.8715 (−1)	−1.6474 (−1)	−4.8632 (−2)	5.4400 (−2)	3.2267 (−2)
8	−5.8573 (−2)	−5.6131 (−2)	−4.4288 (−3)	7.2684 (−2)	4.1359 (−2)
9	6.0592 (−2)	4.0296 (−2)	9.2186 (−3)	4.7889 (−2)	1.1747 (−2)
10	1.1660 (−1)	8.3307 (−2)	−6.4612 (−3)	9.6586 (−3)	−1.7466 (−2)
11	9.8846 (−2)	7.0358 (−2)	−2.7229 (−2)	−1.0687 (−2)	−2.0649 (−2)
12	3.3964 (−2)	2.6471 (−2)	−3.1179 (−2)	−5.3664 (−3)	−2.9665 (−3)
13	−3.4778 (−2)	−1.6224 (−2)	−1.4585 (−2)	1.0427 (−2)	1.3218 (−2)

l \ ρ	1.2	1.5	2.0	5.0	10.0
0	9.0037 (−1)	6.1910 (−1)	3.2580 (−1)	2.4692 (−2)	3.1293 (−3)
1	6.5297 (−1)	3.9677 (−1)	1.6583 (−1)	5.0026 (−3)	3.1407 (−4)
2	2.8932 (−1)	8.8340 (−2)	−3.1552 (−2)	−1.0811 (−2)	−1.5173 (−3)
3	−1.6324 (−2)	−1.2518 (−1)	−1.2927 (−1)	−6.9761 (−3)	−4.6313 (−4)
4	−1.5564 (−1)	−1.8651 (−1)	−8.8713 (−2)	5.6155 (−3)	1.0564 (−3)
5	−1.3742 (−1)	−1.0432 (−1)	1.4583 (−2)	7.6054 (−3)	5.6125 (−4)
6	−5.2771 (−2)	3.1764 (−3)	7.5614 (−2)	−1.8398 (−3)	−7.7684 (−4)
7	6.4034 (−3)	5.2785 (−2)	5.4384 (−2)	−7.1757 (−3)	−6.2568 (−4)
8	7.7352 (−3)	3.7389 (−2)	−6.5513 (−3)	−1.1179 (−3)	5.6176 (−4)
9	−2.1418 (−2)	3.4071 (−3)	−4.2034 (−2)	5.9087 (−3)	6.6240 (−4)
10	−3.8294 (−2)	−7.6326 (−3)	−2.9432 (−2)	3.2646 (−3)	−3.7906 (−4)
11	−2.6571 (−2)	6.0364 (−3)	3.1900 (−3)	−4.0690 (−3)	−6.7448 (−4)
12	−2.4071 (−3)	1.8936 (−2)	1.9108 (−2)	−4.5379 (−3)	2.1756 (−4)
13	1.0215 (−2)	1.3014 (−2)	1.0859 (−2)	1.9591 (−3)	6.6418 (−4)

h=2.0 l \ ρ	0	0.2	0.5	0.8	1.0
0	6.6333 (−1)	6.5663 (−1)	6.2286 (−1)	5.6597 (−1)	5.1954 (−1)
1	6.2832 (−1)	6.2033 (−1)	5.8026 (−1)	5.1359 (−1)	4.6008 (−1)
2	5.6199 (−1)	5.5195 (−1)	5.0190 (−1)	4.2003 (−1)	3.5598 (−1)
3	4.7124 (−1)	4.5928 (−1)	3.9995 (−1)	3.0454 (−1)	2.3208 (−1)
4	3.6529 (−1)	3.5254 (−1)	2.8937 (−1)	1.8915 (−1)	1.1540 (−1)
5	2.5447 (−1)	2.4285 (−1)	1.8488 (−1)	9.2889 (−2)	2.7138 (−2)
6	1.4893 (−1)	1.4073 (−1)	9.8168 (−2)	2.7404 (−2)	−2.2682 (−2)
7	5.7413 (−2)	5.4681 (−2)	3.6001 (−2)	−4.9330 (−3)	−3.6350 (−2)
8	−1.3698 (−2)	−9.7870 (−3)	−3.7792 (−4)	−1.0030 (−2)	−2.5404 (−2)
9	−6.1018 (−2)	−5.0573 (−2)	−1.4595 (−2)	1.1624 (−3)	−4.9948 (−3)
10	−8.4305 (−2)	−6.8873 (−2)	−1.3479 (−2)	1.6821 (−2)	1.1925 (−2)
11	−8.6195 (−2)	−6.8555 (−2)	−4.9232 (−3)	2.7909 (−2)	1.8444 (−2)
12	−7.1549 (−2)	−5.5188 (−2)	4.1327 (−3)	3.0222 (−2)	1.4479 (−2)
13	−4.6553 (−2)	−3.4932 (−2)	9.1247 (−3)	2.4418 (−2)	4.7874 (−3)

l \ ρ	1.2	1.5	2.0	5.0	10.0
0	4.6970 (−1)	3.9438 (−1)	2.8271 (−1)	4.1460 (−2)	5.9847 (−3)
1	4.0376 (−1)	3.2134 (−1)	2.0696 (−1)	1.5787 (−2)	1.1832 (−3)
2	2.9065 (−1)	2.0014 (−1)	8.9034 (−2)	−1.1646 (−2)	−2.6407 (−3)
3	1.6107 (−1)	6.9906 (−2)	−2.1766 (−2)	−1.7831 (−2)	−1.6583 (−3)
4	4.6708 (−2)	−3.2114 (−2)	−8.5503 (−2)	−3.1794 (−3)	1.4056 (−3)
5	−3.0151 (−2)	−8.4575 (−2)	−8.9692 (−2)	1.1935 (−2)	1.8256 (−3)
6	−6.2584 (−2)	−8.7743 (−2)	−5.0978 (−2)	1.0892 (−2)	−5.0880 (−4)
7	−5.8611 (−2)	−5.9240 (−2)	−1.3490 (−3)	−2.4198 (−3)	−1.7496 (−3)
8	−3.5329 (−2)	−2.3059 (−2)	3.1301 (−2)	−1.1062 (−2)	−2.0353 (−4)
9	−1.0687 (−2)	2.0473 (−3)	3.6461 (−2)	−5.7689 (−3)	1.4767 (−3)
10	3.4017 (−3)	9.2652 (−3)	2.1731 (−2)	5.5909 (−3)	7.3707 (−4)
11	4.0067 (−3)	3.2242 (−3)	3.1477 (−3)	9.1154 (−3)	−1.0619 (−3)
12	−4.2982 (−3)	−5.9353 (−3)	−6.8639 (−3)	1.5814 (−3)	−1.0761 (−3)
13	−1.3803 (−2)	−9.7357 (−3)	−5.9984 (−3)	−7.0051 (−3)	5.6923 (−4)

TABLE 1.* *Coefficients $p_l(\rho,h)$ of the Legendre expansion (5) of the angular response function ψ (θ,ρ,h)*—Continued

$p_l(\rho, h)$

h=5.0	l \ ρ	0	0.2	0.5	0.8	1.0
	0	1.2202 (−1)	1.2174 (−1)	1.2033 (−1)	1.1776 (−1)	1.1547 (−1)
	1	1.2083 (−1)	1.2047 (−1)	1.1863 (−1)	1.1530 (−1)	1.1235 (−1)
	2	1.1848 (−1)	1.1797 (−1)	1.1528 (−1)	1.1050 (−1)	1.0628 (−1)
	3	1.1502 (−1)	1.1427 (−1)	1.1041 (−1)	1.0358 (−1)	9.7641 (−2)
	4	1.1051 (−1)	1.0947 (−1)	1.0417 (−1)	9.4882 (−2)	8.6923 (−2)
	5	1.0503 (−1)	1.0368 (−1)	9.6759 (−2)	8.4810 (−2)	7.4740 (−2)
	6	9.8700 (−2)	9.7005 (−2)	8.8421 (−2)	7.3820 (−2)	6.1761 (−2)
	7	9.1627 (−2)	8.9600 (−2)	7.9414 (−2)	6.2393 (−2)	4.8664 (−2)
	8	8.3946 (−2)	8.1617 (−2)	7.0609 (−2)	5.1001 (−2)	3.6090 (−2)
	9	7.5798 (−2)	7.3219 (−2)	6.0477 (−2)	4.0086 (−2)	2.4596 (−2)
	10	6.7330 (−2)	6.4572 (−2)	5.1080 (−2)	3.0033 (−2)	1.4624 (−2)
	11	5.8690 (−2)	5.5842 (−2)	4.2057 (−2)	2.1148 (−2)	6.4728 (−3)
	12	5.0028 (−2)	4.7193 (−2)	3.3619 (−2)	1.3649 (−2)	2.9255 (−4)
	13	4.1487 (−2)	3.8775 (−2)	2.5939 (−2)	7.6574 (−3)	−3.9175 (−3)
	l \ ρ	1.2	1.5	2.0	5.0	10.0
	0	1.1277 (−1)	1.0806 (−1)	9.8893 (−2)	4.4590 (−2)	1.1307 (−2)
	1	1.0889 (−1)	1.0291 (−1)	9.1512 (−2)	3.1724 (−2)	5.0832 (−3)
	2	1.0140 (−1)	9.3079 (−2)	7.7719 (−2)	1.1644 (−2)	−2.2205 (−3)
	3	9.0832 (−2)	7.9469 (−2)	5.9298 (−2)	−7.1460 (−3)	−5.0443 (−3)
	4	7.7933 (−2)	6.3284 (−2)	3.8554 (−2)	−1.7407 (−2)	−2.3029 (−3)
	5	6.3572 (−2)	4.5910 (−2)	1.7958 (−2)	−1.6477 (−2)	2.1603 (−3)
	6	4.8683 (−2)	2.8750 (−2)	−2.3434 (−4)	−7.1132 (−3)	3.6874 (−3)
	7	3.4173 (−2)	1.3078 (−2)	−1.4299 (−2)	4.4049 (−3)	1.2290 (−3)
	8	2.0853 (−2)	−8.7710 (−5)	−2.3258 (−2)	1.1755 (−2)	−2.1739 (−3)
	9	9.3700 (−3)	−1.0080 (−2)	−2.6958 (−2)	1.1721 (−2)	−2.9248 (−3)
	10	1.6819 (−4)	−1.6621 (−2)	−2.6000 (−2)	5.4042 (−3)	−5.4759 (−4)
	11	−6.5366 (−3)	−1.9815 (−2)	−2.1555 (−2)	−2.9324 (−3)	2.1682 (−3)
	12	−1.0753 (−2)	−2.0093 (−2)	−1.5101 (−2)	−8.5369 (−3)	2.3570 (−3)
	13	−1.2692 (−2)	−1.8125 (−2)	−8.1402 (−3)	−8.7686 (−3)	4.6573 (−5)
h=10.0	l \ ρ	0	0.2	0.5	0.8	1.0
	0	3.1182 (−2)	3.1164 (−2)	3.1068 (−2)	3.0890 (−2)	3.0728 (−2)
	1	3.1105 (−2)	3.1081 (−2)	3.0953 (−2)	3.0718 (−2)	3.0504 (−2)
	2	3.0951 (−2)	3.0914 (−2)	3.0725 (−2)	3.0376 (−2)	3.0059 (−2)
	3	3.0720 (−2)	3.0666 (−2)	3.0384 (−2)	2.9869 (−2)	2.9400 (−2)
	4	3.0414 (−2)	3.0337 (−2)	2.9936 (−2)	2.9202 (−2)	2.8539 (−2)
	5	3.0035 (−2)	2.9930 (−2)	2.9382 (−2)	2.8385 (−2)	2.7488 (−2)
	6	2.9584 (−2)	2.9446 (−2)	2.8728 (−2)	2.7429 (−2)	2.6266 (−2)
	7	2.9064 (−2)	2.8889 (−2)	2.7981 (−2)	2.6344 (−2)	2.4889 (−2)
	8	2.8476 (−2)	2.8261 (−2)	2.7145 (−2)	2.5145 (−2)	2.3381 (−2)
	9	2.7825 (−2)	2.7566 (−2)	2.6228 (−2)	2.3848 (−2)	2.1764 (−2)
	10	2.7113 (−2)	2.6808 (−2)	2.5239 (−2)	2.2466 (−2)	2.0063 (−2)
	11	2.6343 (−2)	2.5991 (−2)	2.4184 (−2)	2.1018 (−2)	1.8302 (−2)
	12	2.5520 (−2)	2.5119 (−2)	2.3074 (−2)	1.9520 (−2)	1.6506 (−2)
	13	2.4647 (−2)	2.4198 (−2)	2.1916 (−2)	1.7990 (−2)	1.4702 (−2)
	l \ ρ	1.2	1.5	2.0	5.0	10.0
	0	3.0532 (−2)	3.0176 (−2)	2.9429 (−2)	2.2412 (−2)	1.1118 (−2)
	1	3.0245 (−2)	2.9776 (−2)	2.8801 (−2)	2.0042 (−2)	7.8735 (−3)
	2	2.9677 (−2)	2.8988 (−2)	2.7568 (−2)	1.5688 (−2)	2.8106 (−3)
	3	2.8838 (−2)	2.7832 (−2)	2.5777 (−2)	1.0051 (−2)	−1.9193 (−3)
	4	2.7746 (−2)	2.6336 (−2)	2.3496 (−2)	4.0196 (−3)	−4.4729 (−3)
	5	2.6422 (−2)	2.4540 (−2)	2.0810 (−2)	−1.4972 (−3)	−4.1608 (−3)
	6	2.4890 (−2)	2.2487 (−2)	1.7818 (−2)	−5.7256 (−3)	−1.6836 (−3)
	7	2.3181 (−2)	2.0229 (−2)	1.4627 (−2)	−8.1599 (−3)	1.3314 (−3)
	8	2.1327 (−2)	1.7821 (−2)	1.1348 (−2)	−8.6369 (−3)	3.2194 (−3)
	9	1.9360 (−2)	1.5318 (−2)	8.0921 (−3)	−7.3437 (−3)	3.1141 (−3)
	10	1.7318 (−2)	1.2780 (−2)	4.9635 (−3)	−4.7585 (−3)	1.3036 (−3)
	11	1.5235 (−2)	1.0261 (−2)	2.0567 (−3)	−1.5409 (−3)	−1.0422 (−3)
	12	1.3148 (−2)	7.8155 (−3)	−5.4776 (−4)	1.6059 (−3)	−2.5824 (−3)
	13	1.1089 (−2)	5.4916 (−3)	−2.7864 (−3)	4.0706 (−3)	−2.5433 (−3)

*The figures in parentheses in tables 1, 2, and 3 indicate the power of 10 by which the adjacent entry is to be multiplied; e.g., 2.2831 (−2)=0.022831.

source-plane, table 1 may be used in two different ways:

(a) If the angular distribution data is already in the form of g_l coefficients of a Legendre expansion as given in (4), a new set of coefficients $p'_l(\rho,h)$ may be obtained from the entries in table 1 according to

$$p'_l(\rho,h)=\{lp_{l-1}(\rho,h)+(l+1)p_{l+1}(\rho,h)\}/(2l+1) \qquad (32)$$

which can be combined with the g_l data as in (6).

(b) If the source data are given in terms of the actual angular distribution $g(\theta)$, which could be either a mathematical expression or experimental data, it would be simpler to modify the *source* angular distribution coefficients, that is, to generate Legendre coefficients g'_l of the quantity $g'(\theta)=\cos\theta\, g(\theta)$. These g'_l coefficients could then be combined directly with p_l values from table 1 in the same way as has been specified in (6) for an isotropic detector.

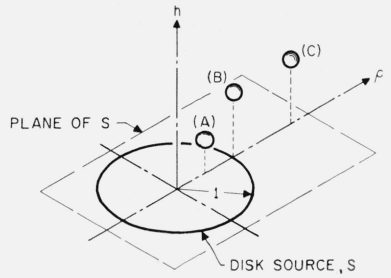

FIGURE 3. *Three examples of detector positions in which the distances off-axis and off source-plane, measured in disk radii, are (A) $\rho=0.5$, $h=0.5$, (B) $\rho=1$, $h=1$ and (C) $\rho=2$, $h=1$.*

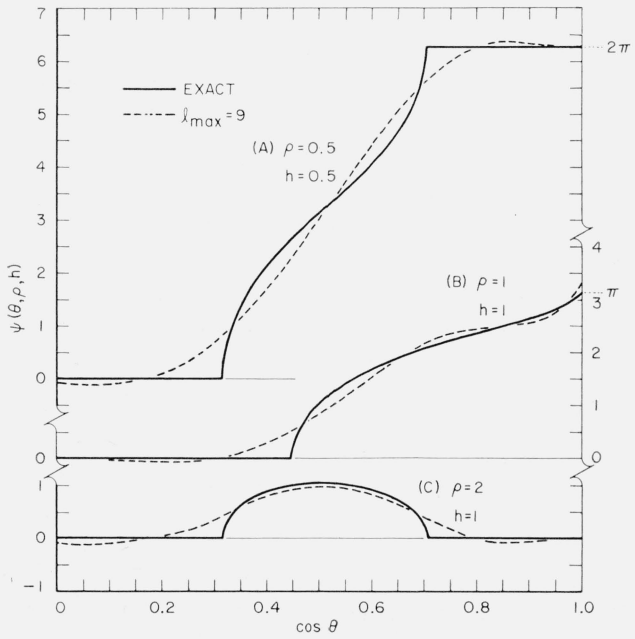

FIGURE 4. *Reconstruction of the response function $\psi(\theta,\rho,h)$ according to (5) for (A) $\rho=.5$, $h=.5$, (B) $\rho=1$, $h=1$ and (C) $\rho=2$, $h=1$ using table 1 and summing over terms $0\leq l\leq 9$. The reconstructed functions are shown as dotted lines and the exact functions as solid lines. Note that the scale for (B) is on the right-hand side.*

2.3. Limitation of the Legendre Expansion Method

The utility of this method is dependent on the oscillatory nature of $P_l(\cos\theta)$. Within any finite region between $\cos\theta$ and $\cos\theta+\Delta\cos\theta$ the increasing number of these oscillations, for increasing l, yields decreasing values of p_l and g_l as a result of higher and higher order cancellations. If both functions $\psi_S(\theta)$ and $g(\theta)$ are concentrated mostly within very *narrow* regions of $\cos\theta$, adequate convergence of (6) may not be achieved without going to exorbitantly high l's.

Evaluation of the unscattered radiation component provides an example of the above limitation. This problem has been qualitatively discussed in section 1, and will be treated in some detail in the following section.

3. Unscattered Radiation Component

3.1. $\tau\gtrsim 1$: Legendre Expansion

As in the rectangular source case [3], the Legendre sum (6) converges adequately for an angular distribution of the form (1) when the barrier thickness $\tau=\mu t$ is of the order of one or greater. In this region the behavior of $g(\theta)$ at the barrier exit surface lies between that of a "perfectly diffuse" plane source $\{g(\theta)=\text{constant}\}$ and that of a plane normal source $\{g(\theta)\propto\delta(\theta-0)\}$. The g_l^o coefficients are easily obtained from appropriate combinations of tabulated exponential integrals [17], and a sample tabulation of g_l^o's is given in reference [3] for $0\leq l\leq 13$ over the range $0.001\leq\tau\leq 100.0$.

3.2. $0\leq\tau\lesssim 1$; $h>0$: Power Series Expansion

Since one of the chief reasons for separate treatment of the unscattered radiation component is the inadequate convergence of (6) for $\tau<<1$, an alternative means of evaluating the integral

$$I^o(\tau,\rho,h)=\frac{\sigma}{4\pi}\int_S (dS/r^2)\,\exp\,(-\tau/\cos\theta) \qquad (33)$$

is desirable. Again, as in [3], no success was had in obtaining a closed-form result for $I^o(\tau,\rho,h)$ in (33). However, Sievert [18] has shown that by expanding $\exp\,(-\tau/\cos\theta)$ as a $(\tau/\cos\theta)^n$ power series, a solution corresponding to eq (10) in reference [3] may be written

$$I^o(\tau,\rho,h)=\frac{\sigma}{4\pi}\sum_{n=0}^{\infty} q_n(\rho,h)\tau^n, \qquad (34)$$

in which the $q_n(\rho,h)$ coefficients are evaluations of the integrals

$$q_n(\rho,h)=\frac{(-1)^n}{n!h^n}\int_{\rho-1}^{\rho+1}(h^2+R^2)^{\frac{n}{2}-1}2\cos^{-1}\left(\frac{\rho^2+R^2}{2\rho R}\right)RdR \qquad (35)$$

for $1\leq\rho\leq\infty$ and

$$q_n(\rho,h)=\frac{(-1)^n}{n!h^n}\left\{\int_0^{1-\rho}(h^2+R^2)^{\frac{n}{2}-1}2\pi RdR\right.$$
$$\left.+\int_{1-\rho}^{1+\rho}(h^2+R^2)^{\frac{n}{2}-1}\,2\cos^{-1}\left(\frac{\rho^2+R^2-1}{2\rho R}\right)RdR\right\} \qquad (36)$$

for $0\leq\rho\leq 1$. As in the $p_l(\rho,h)$ evaluation, three distinct expressions arise from (35) and (36) depending on whether n is zero, even or odd, but by proper manipulation the distinctions between results from (35) and (36) were removed. In reference [18], $q_n(\rho,h)$ coefficients are given only for $n=0$, 1, and 2, of which $q_1(\rho,h)$ is not exact.

The zeroth coefficient $q_0(\rho,h)$, when multiplied by the source strength factor $\sigma/4\pi$, is the radiation field from a disk source in a nonattenuating medium (i.e., $\tau=0$). This can be written, for $h>0$, as [18]

$$q_0(\rho,h)=I^o_{\tau=0}4\pi/\sigma=\pi\ln\{(1+h^2-\rho^2+\sqrt{(1+h^2-\rho^2)^2+4\rho^2h^2})/2h^2\}. \quad (37)$$

Higher even-n terms (i.e., $n(e)=2, 4, 6, \ldots$) are closed-form purely algebraic expressions, the next two of which are

$$q_2(\rho,h)=\frac{\pi}{2!h^2} \quad (38)$$

and

$$q_4(\rho,h)=\frac{\pi}{4!h^4}(h^2+\rho^2+\tfrac{1}{2}). \quad (39)$$

These are included in the general expression for the even-n terms:

$$q_{n(e)}(\rho,h)=\frac{\pi}{n\cdot n!}\left\{-1+\left(\frac{h^2+\rho^2+1}{h^2}\right)^{n/2}\left\{\sum_{i=0}^{i_{\max}\le n/4}\binom{2i}{i}\binom{n/2}{2i}\left(\frac{\rho}{h^2+\rho^2+1}\right)^{2i}+\frac{\rho^2-1}{\rho^2+1}\sum_{i=0}^{i_{\max}\le(n/4-1/2)}\binom{2i}{i}\left(\frac{\rho}{\rho^2+1}\right)^{2i}\left[\left(\frac{h^2}{h^2+\rho^2+1}\right)^{n/2}-\sum_{m=0}^{2i}(-1)^m\binom{n/2}{m}\left(\frac{\rho^2+1}{h^2+\rho^2+1}\right)^m\right]\right\}\right\}. \quad (40)$$

The odd-n terms (i.e., $n(o)=1, 3, 5, \ldots$) are all included in the series-expansion solution

$$q_{n(o)}(\rho,h)=-\frac{\pi}{n\cdot n!}\left\{-1+\left(\frac{h^2+\rho^2+1}{h^2}\right)^{n/2}\left\{\sum_{i=0}^{\infty}\binom{2i}{i}\binom{n/2}{2i}\left(\frac{\rho}{h^2+\rho^2+k}\right)^{2i}+\frac{\rho^2-1}{\rho^2+1}\sum_{i=0}^{\infty}\binom{2i}{i}\left(\frac{\rho}{\rho^2+1}\right)^{2i}\left[\left(\frac{h^2}{h^2+\rho^2+1}\right)^{n/2}-\sum_{m=0}^{2i}(-1)^m\binom{n/2}{m}\left(\frac{\rho^2+1}{h^2+\rho^2+1}\right)^m\right]\right\}\right\}, \quad (41)$$

which strongly resembles (40), except that here the quantities $\binom{n/2}{2i}$ and $\binom{n/2}{m}$ are now coefficients of the *infinite* series expansion of half-integral powers of a binomial [19], i.e.,

$$(1+x)^{n/2}=\sum_{m=0}^{\infty}\binom{n/2}{m}x^m. \quad (42)$$

These are readily generated using the recursion

$$\left.\begin{aligned}&\binom{n/2}{0}=1\\&\binom{n/2}{1}=n/2, \text{ and}\\&\binom{n/2}{m}=-\frac{2(m-1)-n}{2m}\binom{n/2}{m-1},\end{aligned}\right\} \quad (43)$$

which is also valid when $n/2$ is an integer, since $\binom{n/2}{m}$, using (43), is zero for $m>n/2$.

By setting $\rho=0$ in (37), (40) and (41) and substituting the resulting values for $q_n(\rho,h)$ in (34), we find the on-axis unscattered flux to be

$$I^o(0,h)=(\sigma/4\pi)2\pi\left[\ln\frac{\sqrt{h^2+1}}{h}+\sum_{n=1}^{\infty}\frac{(-1)^n}{n\cdot n!}\left\{\left(\frac{\sqrt{h^2+1}}{h}\right)^n-1\right\}\tau^n\right]. \quad (44)$$

This series can be identified with the familiar on-axis solution in terms of exponential integrals [20]

$$I^o(0,h)=(\sigma/4\pi)\int_h^{\sqrt{h^2+1}}\frac{e^{-\mu r}}{r^2}2\pi r dr$$

$$=(\sigma/4\pi)2\pi\{E_1(\tau)-E_1(\tau\sqrt{h^2+1}/h)\}. \quad (45)$$

Equations (37), (40) and (41) were programed for evaluation on an IBM 704 computer and a resulting set of $q_n(\rho,h)$ coefficients for $0\le\rho\le10$, $0.1\le h<10$ and $0\le n\le9$ is given in table 2.

3.3. Comparison of Legendre and Power Series Expansions

As a partial check on tables 1 and 2, and because the unscattered radiation component is of some general interest, the quantities $I^o(\tau,\rho,h)4\pi/\sigma$ as defined in (33) were evaluated using the methods of the preceding two sections, and are given in table 3. Numbers preceded by asterisks were evaluated using the Legendre expansion approach (6) with g^o_l values from reference [3] and $0\le l\le13$; the others are evaluated using the τ^n series (34) for $0\le n\le20$.

Some notion of the convergence for each method may be obtained from table 4, in which partial sums over $0\le l\le13$ and $0\le n\le13$ for $\tau=1.0$ are given for the three situations shown in figure 3. A qualitative comment about the Legendre sums for these three cases is that in each case the first two terms contribute over 80 percent of the result.

For scattered radiation the tendency is toward even faster convergence. For example, the Fermi approximation [21]

$$g(\theta)=(1+\sqrt{3}\cos\theta)/(1+\sqrt{3}/2), \quad (46)$$

used in reference [7] for the angular distribution of neutrons from a reactor thermal-column face, has been shown by Placzek [22] to be in error by less than one percent for $0.1<\cos\theta<1$, with a maximum error of 7.2 percent at $\cos\theta=0$. The Legendre expansion coefficients for the $g(\theta)$ in (46) are: $g_0=1.072$, $g_1=0.6188$ and $g_{l\ge2}=0$, which may be used with the p_l values in table 1 according to (6).

TABLE 2. *Coefficients $q'_n(\rho,h)$ $[=h^n q_n(\rho,h)]$ of the $(\tau/h)^n$ power series expansion (34) of the unscattered component $(4\pi/\sigma)I^o(\tau,\rho,h)$ of the radiation flux, from a circular plane isotropic source, incident on a detector at position ρ,h separated from the source-plane by an attenuating layer of thickness $\tau=\mu t$. Each term contains the factor h^n in order to include meaningful tabulations in the region $\rho>1,h\approx 0$ as in (47).*

$q_n'(\rho,h)=h^n q_n(\rho,h)$

$h=0$	n \ ρ	0	0.2	0.5	0.8	1.0
	0					
	1					
	2					
	3		[No physical solution within the radiating surface.]			
	4					
	5					
	6					
	7					
	8					
	9					
	n \ ρ	1.2	1.5	2.0	5.0	10.0
	0	3.6157 (0)	1.8465 (0)	9.0378 (−1)	1.2825 (−1)	3.1574 (−2)
	1	−2.9533 (0)	−2.2364 (0)	−1.6252 (0)	−6.3151 (−1)	−3.1455 (−1)
	2	1.5708 (0)	1.5708 (0)	1.5708 (0)	1.5708 (0)	1.5708 (0)
	3	−6.8470 (−1)	−8.2992 (−1)	−1.0803 (0)	−2.6311 (0)	−5.2425 (0)
	4	2.5395 (−1)	3.5997 (−1)	5.8905 (−1)	3.3379 (0)	1.3155 (1)
	5	−8.1621 (−2)	−1.3336 (−1)	−2.6896 (−1)	−3.4200 (0)	−2.6475 (1)
	6	2.3069 (−2)	4.3179 (−2)	1.0617 (−1)	2.9467 (0)	4.4507 (1)
	7	−5.8064 (−3)	−1.2414 (−2)	−3.6999 (−2)	−2.1951 (0)	−6.4288 (1)
	8	1.3158 (−3)	3.2080 (−3)	1.1551 (−2)	1.4425 (0)	8.1446 (1)
	9	−2.7095 (−4)	−7.5263 (−4)	−3.2677 (−3)	−8.4902 (−1)	−9.1932 (1)
$h=0.1$	n \ ρ	0	0.2	0.5	0.8	1.0
	0	1.4499 (1)	1.4373 (1)	1.3619 (1)	1.1476 (1)	7.3908 (0)
	1	−5.6862 (0)	−5.6239 (0)	−5.2804 (0)	−4.5455 (0)	−3.7113 (0)
	2	1.5708 (0)	1.5708 (0)	1.5708 (0)	1.5708 (0)	1.5708 (0)
	3	−3.5397 (−1)	−3.6436 (−1)	−4.1803 (−1)	−5.1342 (−1)	−5.9576 (−1)
	4	6.6759 (−2)	7.1995 (−2)	9.9484 (−2)	1.5054 (−1)	1.9766 (−1)
	5	−1.0736 (−2)	−1.2326 (−2)	−2.1058 (−2)	−3.8949 (−2)	−5.7335 (−2)
	6	1.4985 (−3)	1.8581 (−3)	3.9747 (−3)	8.9266 (−3)	1.4676 (−2)
	7	−1.8441 (−4)	−2.5003 (−4)	−6.7332 (−4)	−1.8285 (−3)	−3.3511 (−3)
	8	2.0270 (−5)	3.0378 (−5)	1.0316 (−4)	3.3788 (−4)	6.8960 (−4)
	9	−2.0120 (−6	−3.3635 (−6)	−1.4403 (−5)	−5.6805 (−5)	−1.2903 (−4)
	n \ ρ	1.2	1.5	2.0	5.0	10.0
	0	3.6033 (0)	1.8269 (0)	9.0031 (−1)	1.2819 (−1)	3.1571 (−2)
	1	−2.9136 (0)	−2.2276 (0)	−1.6225 (0)	−6.3138 (−1)	−3.1454 (−1)
	2	1.5708 (0)	1.5708 (0)	1.5708 (0)	1.5708 (0)	1.5708 (0)
	3	−6.8715 (−1)	−8.3178 (−1)	−1.0816 (0)	−2.6316 (0)	−5.2428 (0)
	4	2.5525 (−1)	3.6128 (−1)	5.9036 (−1)	3.3393 (0)	1.3157 (1)
	5	−8.2135 (−2)	−1.3399 (−1)	−2.6977 (−1)	−3.4220 (0)	−2.6479 (1)
	6	2.3238 (−2)	4.3419 (−2)	1.0657 (−1)	2.9489 (0)	4.4516 (1)
	7	−5.8551 (−3)	−1.2493 (−2)	−3.7159 (−2)	−2.1971 (0)	−6.4304 (1)
	8	1.3282 (−3)	3.2312 (−3)	1.1608 (−2)	1.4440 (0)	8.1470 (1)
	9	−2.7379 (−4)	−7.5869 (−4)	−3.2857 (−3)	−8.5009 (−1)	−9.1963 (1)
$h=0.2$	n \ ρ	0	0.2	0.5	0.8	1.0
	0	1.0236 (1)	1.0117 (1)	9.4210 (0)	7.6461 (0)	5.3698 (0)
	1	−5.1510 (0)	−5.0914 (0)	−4.7664 (0)	−4.1033 (0)	−3.4555 (0)
	2	1.5708 (0)	1.5708 (0)	1.5708 (0)	1.5708 (0)	1.5708 (0)
	3	−3.6743 (−1)	−3.7767 (−1)	−4.3050 (−1)	−5.2415 (−1)	−6.0468 (−1)
	4	7.0686 (−2)	7.5922 (−2)	1.0341 (−1)	1.5446 (−1)	2.0159 (−1)
	5	−1.1547 (−2)	−1.3161 (−2)	−2.2013 (−2	−4.0116 (−2)	−5.8685 (−2)
	6	1.6360 (−3)	2.0060 (−3)	4.1776 (−3)	9.2316 (−3)	1.5075 (−2)
	7	−2.0430 (−4)	−2.7278 (−4)	−7.1178 (−4)	−1.8991 (−3)	−3.4547 (−3)
	8	2.2788 (−5)	3.3482 (−5)	1.0971 (−4)	3.5247 (−4)	7.1350 (−4)
	9	−2.2952 (−6)	−3.7445 (−6)	−1.5412 (−5)	−5.9523 (−5)	−1.3399 (−4)
	n \ ρ	1.2	1.5	2.0	5.0	10.0
	0	3.2477 (0)	1.7714 (0)	8.9009 (−1)	1.2803 (−1)	3.1561 (−2)
	1	−2.8313 (0)	−2.2021 (0)	−1.6145 (0)	−6.3098 (−1)	−3.1449 (−1)
	2	1.5708 (0)	1.5708 (0)	1.5708 (0)	1.5708 (0)	1.5708 (0)
	3	−6.9432 (−1)	−8.3732 (−1)	−1.0857 (0)	−2.6332 (0)	−5.2436 (0)
	4	2.5918 (−1)	3.6521 (−1)	5.9429 (−1)	3.3432 (0)	1.3161 (1)
	5	−8.3689 (−2)	−1.3586 (−1)	−2.7221 (−1)	−3.4279 (0)	−2.6490 (1)
	6	2.3753 (−2)	4.4146 (−2)	1.0775 (−1)	2.9556 (0)	4.4542 (1)
	7	−6.0032 (−3)	−1.2734 (−2)	−3.7643 (−2)	−2.2032 (0)	−6.4351 (1)
	8	1.3660 (−3)	3.3015 (−3)	1.1780 (−2)	1.4488 (0)	8.1542 (1)
	9	−2.8243 (−4)	−7.7708 (−4)	−3.3402 (−3)	−8.5330 (−1)	−9.2057 (1)

TABLE 2. *Coefficients $q'_n(\rho,h)$ $[=h^n q_n(\rho,h)]$ of the $(\tau/h)^n$ power series expansion (34) of the unscattered component $(4\pi/\sigma)I^0(\tau,\rho,h)$ of the radiation flux, from a circular plane isotropic source, incident on a detector at position ρ,h separated from the source-plane by an attenuating layer of thickness $\tau=\mu t$. Each term contains the factor h^n in order to include meaningful tabulations in the region $\rho>1,h\approx 0$ as in (47)*—Continued.

$q_n'(\rho,h)=h^n q_n(\rho,h)$

$h=0.5$	n \ ρ	0	0.2	0.5	0.8	1.0
	0	5.0562 (0)	4.9753 (0)	4.5353 (0)	3.6855 (0)	2.9550 (0)
	1	−3.8832 (0)	−3.8383 (0)	−3.6032 (0)	−3.1826 (0)	−2.8363 (0)
	2	1.5708 (0)	1.5708 (0)	1.5708 (0)	1.5708 (0)	1.5708 (0)
	3	−4.4420 (−1)	−4.5354 (−1)	−5.0155 (−1)	−5.8610 (−1)	−6.5868 (−1)
	4	9.8175 (−2)	1.0341 (−1)	1.3090 (−1)	1.8195 (−1)	2.2907 (−1)
	5	−1.7967 (−2)	−1.9734 (−2)	−2.9378 (−2)	−4.8879 (−2)	−6.6468 (−2)
	6	2.8180 (−3)	3.2613 (−3)	5.8178 (−3)	1.1587 (−2)	1.8090 (−2)
	7	−3.8751 (−4)	−4.7714 (−4)	−1.0318 (−3)	−2.4543 (−3)	−4.2497 (−3)
	8	4.7480 (−5)	6.2749 (−5)	1.6557 (−4)	4.6921 (−4)	8.9969 (−4)
	9	−5.2476 (−6)	−7.5023 (−6)	−2.4234 (−5)	−8.1650 (−5)	−1.7321 (−4)
	n \ ρ	1.2	1.5	2.0	5.0	10.0
	0	2.2550 (0)	1.4874 (0)	8.2602 (−1)	1.2690 (−1)	3.1494 (−2)
	1	−2.4916 (0)	−2.0556 (0)	−1.5625 (0)	−6.2825 (−1)	−3.1416 (−1)
	2	1.5708 (0)	1.5708 (0)	1.5708 (0)	1.5708 (0)	1.5708 (0)
	3	−7.4054 (−1)	−8.7450 (−1)	−1.1135 (0)	−2.6442 (0)	−5.2491 (0)
	4	2.8667 (−1)	3.9270 (−1)	6.2177 (−1)	3.3707 (0)	1.3188 (1)
	5	−9.4997 (−2)	−1.4935 (−1)	−2.8953 (−1)	−3.4695 (0)	−2.6573 (1)
	6	2.7574 (−2)	4.9451 (−2)	1.1626 (−1)	3.0026 (0)	4.4727 (1)
	7	−7.1192 (−3)	−1.4516 (−2)	−4.1153 (−2)	−2.2463 (0)	−6.4683 (1)
	8	1.6543 (−3)	3.8277 (−3)	1.3040 (−2)	1.4823 (0)	8.2044 (1)
	9	−3.4929 (−4)	−9.1603 (−4)	−3.7422 (−3)	−8.7601 (−1)	−9.2716 (1)
$h=1.0$	n \ ρ	0	0.2	0.5	0.8	1.0
	0	2.1776 (0)	2.1463 (0)	1.9878 (0)	1.7219 (0)	1.5118 (0)
	1	−2.6026 (0)	−2.5805 (0)	−2.4687 (0)	−2.2805 (0)	−2.1288 (0)
	2	1.5708 (0)	1.5708 (0)	1.5708 (0)	1.5708 (0)	1.5708 (0)
	3	−6.3824 (−1)	−6.4562 (−1)	−6.8363 (−1)	−7.5100 (−1)	−8.0972 (−1)
	4	1.9635 (−1)	2.0159 (−1)	2.2907 (−1)	2.8013 (0)	3.2725 (−1)
	5	−4.8767 (−2)	−5.0998 (−2)	−6.3027 (−2)	−8.6736 (−2)	−1.1015 (−1)
	6	1.0181 (−2)	1.0886 (−2)	1.4817 (−2)	2.3138 (−2)	3.1998 (−2)
	7	−1.8368 (−3)	−2.0161 (−3)	−3.0566 (−3)	−5.4471 (−3)	−8.2091 (−3)
	8	2.9219 (−4)	3.3053 (−4)	5.6368 (−4)	1.1504 (−3)	1.8895 (−3)
	9	−4.1608 (−5)	−4.8702 (−5)	−9.4190 (−5)	−2.2055 (−4)	−3.9469 (−4)
	n \ ρ	1.2	1.5	2.0	5.0	10.0
	0	1.2993 (0)	1.0123 (0)	6.6582 (−1)	1.2302 (−1)	3.1257 (−2)
	1	−1.9698 (0)	−1.7394 (0)	−1.4173 (0)	−6.1877 (−1)	−3.1298 (−1)
	2	1.5708 (0)	1.5708 (0)	1.5708 (0)	1.5708 (0)	1.5708 (0)
	3	−8.7743 (−1)	−9.9202 (−1)	−1.2063 (0)	−2.6832 (0)	−5.2687 (0)
	4	3.8485 (−1)	4.9087 (−1)	7.1995 (−1)	3.4688 (0)	1.3286 (1)
	5	−1.4065 (−1)	−2.0193 (−1)	−3.5482 (−1)	−3.6193 (0)	−2.6869 (1)
	6	4.4362 (−2)	7.1540 (−2)	1.4981 (−1)	3.1736 (0)	4.5389 (1)
	7	−1.2351 (−2)	−2.2333 (−2)	−5.5516 (−2)	−2.4045 (0)	−6.5876 (1)
	8	3.0830 (−3)	6.2418 (−3)	1.8369 (−2)	1.6064 (0)	8.3854 (1)
	9	−6.9802 (−4)	−1.5806 (−3)	−5.4956 (−3)	−9.6077 (−1)	−9.5095 (1)
$h=2.0$	n \ ρ	0	0.2	0.5	0.8	1.0
	0	7.0103 (−1)	6.9603 (−1)	6.7068 (−1)	6.2738 (−1)	5.9133 (−1)
	1	−1.4833 (0)	−1.4777 (0)	−1.4491 (0)	−1.3995 (0)	−1.3572 (0)
	2	1.5708 (0)	1.5708 (0)	1.5708 (0)	1.5708 (0)	1.5708 (0)
	3	−1.1102 (0)	−1.1148 (0)	−1.1391 (0)	−1.1831 (0)	−1.2226 (0)
	4	5.8905 (−1)	5.9428 (−1)	6.2177 (−1)	6.7282 (−1)	7.1995 (−1)
	5	−2.5030 (−1)	−2.5382 (−1)	−2.7251 (−1)	−3.0818 (−1)	−3.4218 (−1)
	6	8.8721 (−2)	9.0473 (−2)	9.9902 (−2)	1.1843 (−1)	1.3672 (−1)
	7	−2.6983 (−2)	−2.7684 (−2)	−3.1511 (−2)	−3.9278 (−2)	−4.7227 (−2)
	8	7.1878 (−3)	7.4236 (−3)	8.7303 (−3)	1.1475 (−2)	1.4395 (−2)
	9	−1.7037 (−3)	−1.7722 (−3)	−2.1583 (−3)	−2.9996 (−3)	−3.9319 (−3)
	n \ ρ	1.2	1.5	2.0	5.0	10.0
	0	5.5179 (−1)	4.8995 (−1)	3.9168 (−1)	1.0970 (−1)	3.0342 (−2)
	1	−1.3098 (0)	−1.2327 (0)	−1.1012 (0)	−5.8485 (−1)	−3.0839 (−1)
	2	1.5708 (0)	1.5708 (0)	1.5708 (0)	1.5708 (0)	1.5708 (0)
	3	−1.2693 (0)	−1.3517 (0)	−1.5157 (0)	−2.8335 (0)	−5.3464 (0)
	4	7.7754 (−1)	8.8357 (−1)	1.1127 (0)	3.8615 (0)	1.3679 (1)
	5	−3.8510 (−1)	−4.6789 (−1)	−6.6249 (−1)	−4.2401 (0)	−2.8063 (1)
	6	1.6060 (−1)	2.0899 (−1)	3.3307 (−1)	3.9066 (0)	4.8085 (1)
	7	−5.7991 (−2)	−8.0941 (−2)	−1.4532 (−1)	−3.1058 (0)	−7.0780 (1)
	8	1.8501 (−2)	2.7732 (−2)	5.6119 (−2)	2.1742 (0)	9.1364 (1)
	9	−5.2954 (−3)	−8.5329 (−3)	−1.9471 (−2)	−1.3612 (0)	−1.0506 (2)

TABLE 2. *Coefficients* $q'_n(\rho,h)$ $[=h^n q_n(\rho,h)]$ *of the* $(\tau/h)^n$ *power series expansion (34) of the unscattered component* $(4\pi/\sigma)\, I^o(\tau,\rho,h)$ *of the radiation flux, from a circular plane isotropic source, incident on a detector at position* ρ,h *separated from the source-plane by an attenuating layer of thickness* $\tau=\mu t$. *Each term contains the factor* h^n *in order to include meaningful tabulations in the regular* $\rho>1, h\approx 0$ *as in (47)*—Continued

$q_n'(\rho,h)=h^n q_n(\rho,h)$

$h=5.0$	n \ ρ	0	0.2	0.5	0.8	1.0
	0	1.2322 (−1)	1.2303 (−1)	1.2206 (−1)	1.2031 (−1)	1.1873 (−1)
	1	−6.2216 (−1)	−6.2168 (−1)	−6.1922 (−1)	−6.1471 (−1)	−6.1063 (−1)
	2	1.5708 (0)	1.5708 (0)	1.5708 (0)	1.5708 (0)	1.5708 (0)
	3	−2.6440 (0)	−2.6461 (0)	−2.6568 (0)	−2.6767 (0)	−2.6949 (0)
	4	3.3379 (0)	3.3432 (0)	3.3707 (0)	3.4217 (0)	3.4688 (0)
	5	−3.3713 (0)	−3.3793 (0)	−3.4215 (0)	−3.5003 (0)	−3.5735 (0)
	6	2.8376 (0)	2.8467 (0)	2.8946 (0)	2.9846 (0)	3.0689 (0)
	7	−2.0473 (0)	−2.0555 (0)	−2.0993 (0)	−2.1820 (0)	−2.2599 (0)
	8	1.2925 (0)	1.2988 (0)	1.3324 (0)	1.3962 (0)	1.4568 (0)
	9	−7.2531 (−1)	−7.2949 (−1)	−7.5174 (−1)	−7.9429 (−1)	−8.3502 (−1)
	n \ ρ	1.2	1.5	2.0	5.0	10.0
	0	1.1686 (−1)	1.1355 (−1)	1.0699 (−1)	6.2828 (−2)	2.5193 (−2)
	1	−6.0574 (−1)	−5.9704 (−1)	−5.7943 (−1)	−4.4372 (−1)	−2.8111 (−1)
	2	1.5708 (0)	1.5708 (0)	1.5708 (0)	1.5708 (0)	1.5708 (0)
	3	−2.7170 (0)	−2.7572 (0)	−2.8422 (0)	−3.7163 (0)	−5.8610 (0)
	4	3.5264 (0)	3.6325 (0)	3.8615 (0)	6.6104 (0)	1.6428 (1)
	5	−3.6636 (0)	−3.8314 (0)	−4.2021 (0)	−9.4298 (0)	−3.6895 (1)
	6	3.1734 (0)	3.3702 (0)	3.8150 (0)	1.1237 (1)	6.9160 (1)
	7	−2.3574 (0)	−2.5430 (0)	−2.9723 (0)	−1.1505 (1)	−1.1130 (2)
	8	1.5331 (0)	1.6802 (0)	2.0286 (0)	1.0332 (1)	1.5695 (2)
	9	−8.8671 (−1)	−9.8760 (−1)	−1.2322 (0)	−8.2664 (0)	−1.9705 (2)
$h=10.0$	n \ ρ	0	0.2	0.5	0.8	1.0
	0	3.1260 (−2)	3.1248 (−2)	3.1183 (−2)	3.1064 (−2)	3.0955 (−2)
	1	−3.1338 (−1)	−3.1332 (−1)	−3.1299 (−1)	−3.1239 (−1)	−3.1184 (−1)
	2	1.5708 (0)	1.5708 (0)	1.5708 (0)	1.5708 (0)	1.5708 (0)
	3	−5.2491 (0)	−5.2501 (0)	−5.2556 (0)	−5.2657 (0)	−5.2750 (0)
	4	1.3155 (1)	1.3161 (1)	1.3188 (1)	1.3239 (1)	1.3286 (1)
	5	−2.6377 (1)	−2.6392 (1)	−2.6475 (1)	−2.6630 (1)	−2.6772 (1)
	6	4.4071 (1)	4.4106 (1)	4.4292 (1)	4.4637 (1)	4.4957 (1)
	7	−6.3116 (1)	−6.3180 (1)	−6.3512 (1)	−6.4133 (1)	−6.4710 (1)
	8	7.9093 (1)	7.9188 (1)	7.9691 (1)	8.0629 (1)	8.1501 (1)
	9	−8.8102 (1)	−8.8226 (1)	−8.8881 (1)	−9.0106 (1)	−9.1247 (1)
	n \ ρ	1.2	1.5	2.0	5.0	10.0
	0	3.0823 (−2)	3.0582 (−2)	3.0074 (−2)	2.5072 (−2)	1.5708 (−2)
	1	−3.1117 (−1)	−3.0995 (−1)	−3.0736 (−1)	−2.8060 (−1)	−2.2207 (−1)
	2	1.5708 (0)	1.5708 (0)	1.5708 (0)	1.5708 (0)	1.5708 (0)
	3	−5.2864 (0)	−5.3073 (0)	−5.3522 (0)	−5.8645 (0)	−7.4117 (0)
	4	1.3344 (1)	1.3450 (1)	1.3679 (1)	1.6428 (1)	2.6245 (1)
	5	−2.6947 (1)	−2.7270 (1)	−2.7971 (1)	−3.6829 (1)	−7.4395 (1)
	6	4.5349 (1)	4.6076 (1)	4.7666 (1)	6.8833 (1)	1.7584 (2)
	7	−6.5419 (1)	−6.6735 (1)	−6.9633 (1)	−1.1031 (2)	−3.5647 (2)
	8	8.2576 (1)	8.4579 (1)	8.9016 (1)	1.5475 (2)	6.3271 (2)
	9	−9.2656 (1)	−9.5289 (1)	−1.0116 (2)	−1.9305 (2)	−9.9885 (2)

TABLE 3. *Unscattered component* $(4\pi/\sigma)I^\circ(\tau,\rho,h)$ *of the radiation flux calculated (a) using table 1 of this work and table 2 of reference [3] (numbers preceded by asterisks) and (b) using table 2 of this work (no asterisks).*

$(4\pi/\sigma)\ I^\circ\ (\tau,\ \rho,\ h)$

$h=0.1$	τ \ ρ	0	0.2	0.5	0.8	1.0	1.2	1.5	2.0	5.0	10.0
	0	1.45 (1)	1.44 (1)	1.36 (1)	1.15 (1)	7.39 (0)	3.60 (0)	1.83 (0)	9.00 (−1)	1.28 (−1)	3.16 (−2)
	0.01	1.39 (1)	1.38 (1)	1.31 (1)	1.10 (1)	7.03 (0)	3.33 (0)	1.62 (0)	7.53 (−1)	7.84 (−2)	1.17 (−2)
	0.02	1.34 (1)	1.33 (1)	1.26 (1)	1.06 (1)	6.71 (0)	3.08 (0)	1.44 (0)	6.31 (−1)	4.81 (−2)	4.31 (−3)
	0.05	1.20 (1)	1.19 (1)	1.13 (1)	9.54 (0)	5.86 (0)	2.47 (0)	1.02 (0)	3.76 (−1)	1.13 (−2)	
	0.1	1.01 (1)	1.00 (1)	9.57 (0)	8.11 (0)	4.81 (0)	1.76 (0)	5.99 (−1)	1.66 (−1)		
		*1.00 (1)	*9.98 (0)	*9.56 (0)	*8.02 (0)	*4.72 (0)	*1.65 (0)				
	0.2	7.38 (0)	7.34 (0)	7.10 (0)	6.12 (0)	3.45 (0)	9.94 (−1)				
		*7.27 (0)	*7.24 (0)	*7.04 (0)	*6.07 (0)	*3.41 (0)	*9.38 (−1)	*2.09 (−1)	*4.56 (−2)	*1.36 (−3)	*1.34 (−4)
	0.5	*3.50 (0)	*3.50 (0)	*3.46 (0)	*3.17 (0)	*1.66 (0)	*2.51 (−1)	*2.74 (−2)	*3.45 (−3)	*2.17 (−5)	*1.72 (−5)
	1.0	*1.38 (0)	*1.38 (0)	*1.38 (0)	*1.32 (0)	*6.63 (−1)	*4.25 (−2)	*1.03 (−3)	*2.49 (−4)		
	2.0	*3.08 (−1)	*3.08 (−1)	*3.08 (−1)	*3.05 (−1)	*1.49 (−1)	*2.11 (−3)				
	5.0	*7.22 (−3)	*7.22 (−3)	*7.21 (−3)	*7.21 (−3)	*3.54 (−3)					
	10.0	*2.61 (−5)	*2.61 (−5)	*2.61 (−5)	*2.61 (−5)	*1.29 (−5)					

TABLE 3. *Unscattered component $(4\pi/\sigma)I^{\circ}(\tau,\rho,h)$ of the radiation flux calculated (a) using table 1 of this work and table 2 of reference [3] (numbers preceded by asterisks) and (b) using table 2 of this work (no asterisks)*—Continued

$(4\pi/\sigma)\ I^{\circ}\ (\tau,\ \rho,\ h)$

$h=0.2$	τ \ ρ	0	0.2	0.5	0.8	1.0	1.2	1.5	2.0	5.0	10.0
	0	1.02 (1)	1.01 (1)	9.42 (0)	7.65 (0)	5.37 (0)	3.25 (0)	1.77 (0)	8.90 (−1)	1.28 (−1)	3.16 (−2)
	0.01	9.98 (0)	9.87 (0)	9.19 (0)	7.44 (0)	5.20 (0)	3.11 (0)	1.67 (0)	8.13 (−1)	1.00 (−1)	1.92 (−2)
	0.02	9.74 (0)	9.62 (0)	8.96 (0)	7.25 (0)	5.04 (0)	2.98 (0)	1.57 (0)	7.43 (−1)	7.83 (−2)	1.17 (−2)
	0.05	9.04 (0)	8.94 (0)	8.32 (0)	6.71 (0)	4.60 (0)	2.63 (0)	1.31 (0)	5.70 (−1)	3.76 (−2)	2.63 (−3)
	0.1	8.01 (0)	7.92 (0)	7.38 (0)	5.93 (0)	3.97 (0)	2.15 (0)	9.78 (−1)	3.70 (−1)	1.12 (−2)	1.01 (−3)
	0.2	6.35 (0)	6.28 (0)	5.88 (0)	4.71 (0)	3.17 (0)	1.49 (0)	5.66 (−1)	1.62 (−1)		
		*6.39 (0)	*6.36 (0)	*5.88 (0)	*4.70 (0)	*3.02 (0)	*1.46 (0)	*5.36 (−1)	*1.38 (−1)	*3.48 (−3)	*3.16 (−4)
	0.5	3.37 (0)	3.35 (0)	3.19 (0)	2.60 (0)	1.55 (0)					
		*3.36 (0)	*3.34 (0)	*3.19 (0)	*2.58 (0)	*1.55 (0)	*5.79 (−1)	*1.37 (−1)	*2.19 (−2)	*1.62 (−4)	*4.90 (−6)
	1.0	*1.37 (0)	*1.37 (0)	*1.34 (0)	*1.14 (0)	*6.35 (−1)	*1.67 (−1)	*1.73 (−2)	*1.02 (−3)		
	2.0	*3.08 (−1)	*3.08 (−1)	*3.06 (−1)	*2.80 (−1)	*1.42 (−1)	*2.06 (−2)	*5.93 (−4)			
	5.0	*7.22 (−3)	*7.22 (−3)	*7.21 (−3)	*7.08 (−3)	*3.48 (−3)	*1.04 (−4)	*7.67 (−7)			
	10.0	*2.61 (−5)	*2.61 (−5)	*2.61 (−5)	*2.61 (−5)	*1.27 (−5)	*2.71 (−8)				

$h=0.5$	τ \ ρ	0	0.2	0.5	0.8	1.0	1.2	1.5	2.0	5.0	10.0
	0	5.06 (0)	4.98 (0)	4.53 (0)	3.69 (0)	2.96 (0)	2.26 (0)	1.49 (0)	8.26 (−1)	1.27 (−1)	3.15 (−2)
	0.01	4.98 (0)	4.90 (0)	4.46 (0)	3.62 (0)	2.90 (0)	2.21 (0)	1.45 (0)	7.95 (−1)	1.15 (−1)	2.58 (−2)
	0.02	4.90 (0)	4.82 (0)	4.39 (0)	3.56 (0)	2.84 (0)	2.16 (0)	1.41 (0)	7.66 (−1)	1.04 (−1)	2.11 (−2)
	0.05	4.68 (0)	4.61 (0)	4.19 (0)	3.38 (0)	2.69 (0)	2.02 (0)	1.30 (0)	6.84 (−1)	7.74 (−2)	1.16 (−2)
	0.1	4.34 (0)	4.27 (0)	3.87 (0)	3.11 (0)	2.45 (0)	1.81 (0)	1.13 (0)	5.68 (−1)	4.74 (−2)	4.30 (−3)
	0.2	3.73 (0)	3.66 (0)	3.32 (0)	2.63 (0)	2.03 (0)	1.47 (0)	8.69 (−1)	3.94 (−1)	1.79 (−2)	
	0.5	2.38 (0)	2.34 (0)	2.11 (0)	1.63 (0)	1.21 (0)	8.07 (−1)	4.09 (−1)	1.38 (−1)		
		*2.38 (0)	*2.34 (0)	*2.11 (0)	*1.63 (0)	*1.21 (0)	*8.07 (−1)	*4.08 (−1)	*1.36 (−1)	*1.72 (−3)	6.69 (−5)
	1.0	1.16 (0)	1.14 (0)	1.03 (0)	7.78 (−1)	5.43 (−1)	3.26 (−1)				
		*1.16 (0)	*1.14 (0)	*1.03 (0)	*7.77 (−1)	*5.43 (−1)	*3.26 (−1)	*1.30 (−1)	*2.73 (−2)	*1.87 (−5)	
	2.0	*2.93 (−1)	*2.90 (−1)	*2.69 (−1)	*2.03 (−1)	*1.32 (−1)	*6.64 (−2)	*1.73 (−2)	*1.62 (−3)		
	5.0	*7.21 (−3)	*7.20 (−3)	*7.04 (−3)	*5.76 (−3)	*3.29 (−3)	*1.09 (−3)	*9.00 (−5)	*6.03 (−7)		
	10.0	*2.61 (−5)	*2.61 (−5)	*2.61 (−5)	*2.31 (−5)	*1.22 (−5)	*2.29 (−6)	*2.52 (−8)			

$h=1.0$	τ \ ρ	0	0.2	0.5	0.8	1.0	1.2	1.5	2.0	5.0	10.0
	0	2.18 (0)	2.15 (0)	1.99 (0)	1.72 (0)	1.51 (0)	1.30 (0)	1.01 (0)	6.66 (−1)	1.23 (−1)	3.13 (−2)
	0.01	2.15 (0)	2.12 (0)	1.96 (0)	1.70 (0)	1.49 (0)	1.26 (0)	9.95 (−1)	6.52 (−1)	1.17 (−1)	2.83 (−2)
	0.02	2.13 (0)	2.10 (0)	1.94 (0)	1.68 (0)	1.47 (0)	1.20 (0)	9.78 (−1)	6.38 (−1)	1.11 (−1)	2.56 (−2)
	0.05	2.05 (0)	2.02 (0)	1.87 (0)	1.61 (0)	1.41 (0)	1.20 (0)	9.29 (−1)	5.99 (−1)	9.57 (−2)	1.90 (−2)
	0.1	1.93 (0)	1.90 (0)	1.76 (0)	1.51 (0)	1.31 (0)	1.12 (0)	8.53 (−1)	5.39 (−1)	7.45 (−2)	1.15 (−2)
	0.2	1.71 (0)	1.69 (0)	1.55 (0)	1.32 (0)	1.14 (0)	9.62 (−1)	7.20 (−1)	4.37 (−1)	4.52 (−2)	4.24 (−3)
	0.5	1.20 (0)	1.18 (0)	1.07 (0)	8.96 (−1)	7.56 (−1)	6.18 (−1)	4.37 (−1)	2.35 (−1)	1.02 (−2)	
		*1.21 (0)	*1.18 (0)	*1.07 (0)	*8.94 (−1)	*7.55 (−1)	*6.17 (−1)	*4.37 (−1)	*2.42 (−1)	*9.31 (−3)	*3.96 (−4)
	1.0	6.64 (−1)	6.51 (−1)	5.85 (−1)	4.73 (−1)	3.87 (−1)	3.02 (−1)	1.95 (−1)	8.65 (−2)		
		*6.64 (−1)	*6.51 (−1)	*5.84 (−1)	*4.73 (−1)	*3.87 (−1)	*3.04 (−1)	*1.95 (−1)	*8.65 (−2)	*1.06 (−3)	*2.27 (−6)
	2.0	2.05 (−1)	2.01 (−1)	1.77 (−1)	1.37 (−1)						
		*2.06 (−1)	*2.01 (−1)	*1.77 (−1)	*1.38 (−1)	*1.06 (−1)	*7.67 (−2)	*4.22 (−2)	*1.29 (−2)	*6.65 (−6)	
	5.0	*6.54 (−3)	*6.42 (−3)	*5.76 (−3)	*4.21 (−3)	*2.95 (−3)	*1.79 (−3)	*6.51 (−4)	*7.40 (−5)		
	10.0	*2.58 (−5)	*2.56 (−5)	*2.41 (−5)	*1.78 (−5)	*1.14 (−5)	*5.57 (−6)	*1.13 (−6)	*2.66 (−8)		

$h=2.0$	τ \ ρ	0	0.2	0.5	0.8	1.0	1.2	1.5	2.0	5.0	10.0
	0	7.01 (−1)	6.96 (−1)	6.71 (−1)	6.27 (−1)	5.91 (−1)	5.52 (−1)	4.90 (−1)	3.92 (−1)	1.10 (−1)	3.03 (−2)
	0.01	6.94 (−1)	6.89 (−1)	6.63 (−1)	6.20 (−1)	5.85 (−1)	5.45 (−1)	4.84 (−1)	3.86 (−1)	1.07 (−1)	2.88 (−2)
	0.02	6.86 (−1)	6.81 (−1)	6.56 (−1)	6.14 (−1)	5.78 (−1)	5.39 (−1)	4.78 (−1)	3.81 (−1)	1.04 (−1)	2.74 (−2)
	0.05	6.65 (−1)	6.60 (−1)	6.35 (−1)	5.93 (−1)	5.58 (−1)	5.20 (−1)	4.60 (−1)	3.65 (−1)	9.60 (−2)	2.35 (−2)
	0.1	6.31 (−1)	6.26 (−1)	6.02 (−1)	5.61 (−1)	5.27 (−1)	4.90 (−1)	4.32 (−1)	3.40 (−1)	8.40 (−2)	1.83 (−2)
	0.2	5.67 (−1)	5.63 (−1)	5.40 (−1)	5.02 (−1)	4.70 (−1)	4.35 (−1)	3.81 (−1)	2.96 (−1)	6.44 (−2)	1.10 (−2)
	0.5	4.13 (−1)	4.09 (−1)	3.91 (−1)	3.60 (−1)	3.34 (−1)	3.05 (−1)	2.62 (−1)	1.95 (−1)	2.91 (−2)	2.41 (−3)
		*4.14 (−1)	*4.10 (−1)	*3.90 (−1)	*3.59 (−1)	*3.34 (−1)	*3.07 (−1)	*2.62 (−1)	*1.95 (−1)	*3.00 (−2)	*2.18 (−3)
	1.0	2.44 (−1)	2.41 (−1)	2.28 (−1)	2.06 (−1)	1.89 (−1)	1.70 (−1)	1.41 (−1)	9.74 (−2)	7.83 (−3)	
		*2.43 (−1)	*2.41 (−1)	*2.28 (−1)	*2.07 (−1)	*1.89 (−1)	*1.70 (−1)	*1.40 (−1)	*9.74 (−2)	*7.69 (−3)	*2.35 (−4)
	2.0	8.47 (−2)	8.36 (−2)	7.79 (−2)	6.85 (−2)	6.09 (−2)	5.29 (−2)	4.12 (−2)			
		*8.44 (−2)	*8.33 (−2)	*7.79 (−2)	*6.85 (−2)	*6.09 (−2)	*5.29 (−2)	*4.12 (−2)	*2.50 (−2)	*6.16 (−4)	
	5.0	*3.59 (−3)	*3.52 (−3)	*3.17 (−3)	*2.60 (−3)	*2.16 (−3)	*1.72 (−3)	*1.14 (−3)	*4.77 (−4)	*2.28 (−7)	
	10.0	*1.89 (−5)	*1.84 (−5)	*1.61 (−5)	*1.24 (−5)	*9.55 (−6)	*6.86 (−6)	*3.45 (−6)	*9.02 (−7)		

TABLE 3. *Unscattered component* $(4\pi/\sigma)I^\circ(\tau,\rho,h)$ *of the radiation flux calculated (a) using table 1 of this work and table 2 of reference [3] (numbers preceded by asterisks) and (b) using table 2 of this work (no asterisks)*—Continued

$(4\pi/\sigma)\ I^\circ\ (\rho,\ h,\ \tau)$

$h=5.0$ τ \ ρ	0	0.2	0.5	0.8	1.0	1.2	1.5	2.0	5.0	10.0
0	1.23 (−1)	1.23 (−1)	1.22 (−1)	1.20 (−1)	1.19 (−1)	1.17 (−1)	1.14 (−1)	1.07 (−1)	6.28 (−2)	2.52 (−2)
0.01	1.22 (−1)	1.22 (−1)	1.21 (−1)	1.19 (−1)	1.18 (−1)	1.16 (−1)	1.12 (−1)	1.06 (−1)	6.27 (−2)	2.51 (−2)
0.02	1.21 (−1)	1.21 (−1)	1.20 (−1)	1.18 (−1)	1.16 (−1)	1.14 (−1)	1.11 (−1)	1.05 (−1)	6.11 (−2)	2.41 (−2)
0.05	1.17 (−1)	1.17 (−1)	1.16 (−1)	1.14 (−1)	1.13 (−1)	1.11 (−1)	1.08 (−1)	1.01 (−1)	5.85 (−2)	2.25 (−2)
0.1	1.11 (−1)	1.11 (−1)	1.10 (−1)	1.09 (−1)	1.07 (−1)	1.05 (−1)	1.02 (−1)	9.60 (−2)	5.46 (−2)	2.02 (−2)
0.2	1.01 (−1)	1.01 (−1)	9.96 (−2)	9.81 (−2)	9.66 (−2)	9.50 (−2)	9.20 (−2)	8.62 (−2)	4.74 (−2)	1.61 (−2)
0.5	7.44 (−2)	7.43 (−2)	7.35 (−2)	7.22 (−2)	7.10 (−2)	6.96 (−2)	6.71 (−2)	6.23 (−2)	3.10 (−2)	8.26 (−3)
	*7.24 (−2)	*7.24 (−2)	*7.24 (−2)	*7.20 (−2)	*7.14 (−2)	*7.03 (−2)	*6.80 (−2)	*6.24 (−2)	*3.14 (−2)	*8.50 (−3)
1.0	4.49 (−2)	4.48 (−2)	4.43 (−2)	4.33 (−2)	4.25 (−2)	4.14 (−2)	3.97 (−2)	3.62 (−2)	1.53 (−2)	2.71 (−3)
	*4.50 (−2)	*4.49 (−2)	*4.44 (−2)	*4.33 (−2)	*4.25 (−2)	*4.14 (−2)	*3.96 (−2)	*3.62 (−2)	*1.53 (−2)	*2.72 (−3)
2.0	1.64 (−2)	1.63 (−2)	1.60 (−2)	1.56 (−2)	1.52 (−2)	1.47 (−2)	1.39 (−2)	1.23 (−2)	3.76 (−3)	
	*1.66 (−2)	*1.66 (−2)	*1.62 (−2)	*1.57 (−2)	*1.52 (−2)	*1.47 (−2)	*1.38 (−2)	*1.22 (−2)	*3.77 (−3)	*2.94 (−4)
5.0	*7.91 (−4)	*7.87 (−4)	*7.66 (−4)	*7.29 (−4)	*6.97 (−4)	*6.60 (−4)	*5.97 (−4)	*4.83 (−4)	*5.71 (−5)	*3.77 (−7)
10.0	*5.09 (−6)	*5.05 (−6)	*4.83 (−6)	*4.45 (−6)	*4.13 (−6)	*3.78 (−6)	*3.20 (−6)	*2.27 (−6)	*5.99 (−8)	

$h=10.0$ τ \ ρ	0	0.2	0.5	0.8	1.0	1.2	1.5	2.0	5.0	10.0
0	3.13 (−2)	3.12 (−2)	3.12 (−2)	3.11 (−2)	3.10 (−2)	3.08 (−2)	3.06 (−2)	3.01 (−2)	2.51 (−2)	1.57 (−2)
0.01	3.09 (−2)	3.09 (−2)	3.09 (−2)	3.08 (−2)	3.06 (−2)	3.05 (−2)	3.03 (−2)	2.98 (−2)	2.48 (−2)	1.55 (−2)
0.02	3.06 (−2)	3.06 (−2)	3.06 (−2)	3.04 (−2)	3.03 (−2)	3.02 (−2)	3.00 (−2)	2.95 (−2)	2.45 (−2)	1.53 (−2)
0.05	2.97 (−2)	2.97 (−2)	2.97 (−2)	2.95 (−2)	2.94 (−2)	2.93 (−2)	2.91 (−2)	2.86 (−2)	2.37 (−2)	1.46 (−2)
0.1	2.83 (−2)	2.83 (−2)	2.82 (−2)	2.81 (−2)	2.80 (−2)	2.79 (−2)	2.76 (−2)	2.72 (−2)	2.24 (−2)	1.36 (−2)
0.2	2.56 (−2)	2.56 (−2)	2.55 (−2)	2.54 (−2)	2.53 (−2)	2.52 (−2)	2.50 (−2)	2.45 (−2)	2.00 (−2)	1.18 (−2)
0.5	1.89 (−2)	1.89 (−2)	1.89 (−2)	1.88 (−2)	1.87 (−2)	1.86 (−2)	1.84 (−2)	1.80 (−2)	1.43 (−2)	7.75 (−3)
	*1.76 (−2)	*1.76 (−2)	*1.77 (−2)	*1.79 (−2)	*1.80 (−2)	*1.81 (−2)	*1.82 (−2)	*1.83 (−2)	*1.40 (−2)	*7.86 (−3)
1.0	1.15 (−2)	1.15 (−2)	1.14 (−2)	1.14 (−2)	1.13 (−2)	1.12 (−2)	1.11 (−2)	1.08 (−2)	8.20 (−3)	3.82 (−3)
	*1.15 (−2)	*1.15 (−2)	*1.15 (−2)	*1.14 (−2)	*1.13 (−2)	*1.13 (−2)	*1.11 (−2)	*1.08 (−2)	*8.20 (−3)	*3.80 (−3)
2.0	4.21 (−3)	4.21 (−3)	4.19 (−3)	4.16 (−3)	4.13 (−3)	4.09 (−3)	4.03 (−3)	3.90 (−3)	2.68 (−3)	9.31 (−4)
	*4.33 (−3)	*4.32 (−3)	*4.30 (−3)	*4.25 (−3)	*4.21 (−3)	*4.16 (−3)	*4.08 (−3)	*3.91 (−3)	*2.67 (−3)	*9.33 (−4)
5.0	*2.08 (−4)	*2.08 (−4)	*2.06 (−4)	*2.04 (−4)	*2.04 (−4)	*2.01 (−4)	*1.93 (−4)	*1.82 (−4)	*9.37 (−5)	*1.36 (−5)
10.0	*1.39 (−6)	*1.38 (−6)	*1.37 (−6)	*1.34 (−6)	*1.31 (−6)	*1.28 (−6)	*1.22 (−6)	*1.10 (−6)	*3.53 (−7)	*1.26 (−8)

TABLE 4. *Comparison of convergence in calculating the unscattered component* $(4\pi/\sigma)I^\circ(\tau,\rho,h)$ *in the case* $\tau=\mu t=1$, *for the three situations (A), (B), and (C) indicated in figure 3. For each situation the first column contains partial sums*

$$\sum_{l=0}^{L}(l+\tfrac{1}{2})g_l(\tau)p_l(\rho,h)$$

and the second column contains sums

$$\sum_{n=0}^{N}q_n(\rho,h)\tau^n.$$

L,N	(A): $\rho=0.5$, $h=0.5$		(B): $\rho=1$, $h=1$		(C): $\rho=2$, $h=1$	
	Legendre sum	τ^n-series sum	Legendre sum	τ^n-series sum	Legendre sum	τ^n-series sum
0	0.34031	4.5353	0.12316	1.5118	0.035740	0.66582
1	.84669	−2.6711	.31658	−0.6170	.072679	−0.75149
2	.99567	3.6122	.38273	0.9538	.068353	0.81932
3	.99211	−0.4003	.37916	.1441	.071785	−0.38701
4	1.01738	1.6941	.38475	.4713	.080105	0.33294
5	1.02484	0.7540	.38774	.3612	.079609	−0.02187
6	1.02365	1.1264	.38665	.3932	.082707	0.12793
7	1.02628	0.9943	.38793	.3850	.084872	.07242
8	1.02590	1.0367	.38753	.3869	.084935	.09079
9	1.02615	1.0243	.38718	.3865	.086201	.08529
10	1.02619	1.0276	.38727	.3865	.086348	.08679
11	1.02655	1.0268	.38688	.3865	.086408	.08641
12	1.02677	1.0270	.38685	.3865	.086602	.08650
13	1.02685	1.0269	.38672	.3865	.086496	.08648

A physical interpretation of the rather wild oscillations in the first few terms of the τ^n series is that the zeroth term would be the result for a bare disk source ($\tau=0$), from which the radiation absorbed in the barrier of thickness τ must be subtracted. This subtraction is accomplished by a succession of undershoots and overshoots which are quickly damped out if τ is small enough.

3.4. $h\approx 0$, $\rho>1$: Power Series Solution In or Near Plane of Disk

If both source and detector are embedded in a homogeneous attenuating medium, the series (34) is valid except for $h=0$, where the concept of "barrier thickness" τ becomes meaningless. As $h\to 0$, $q_n\to\infty$ as $1/h^n$, but at the same time $\tau^n\to 0$ as h^n, while $q_0(\rho,0)$ is a finite but indeterminate quantity of the form $\{\infty-\infty\}$.

The series (34) can still be used if the indeterminacy is removed from the product $q_n\tau^n$ by multiplying and dividing q_n and τ^n, respectively, by h^n, resulting in a series of the form

$$I^\circ(\tau,\rho,h)=(\sigma/4\pi)\sum_{n=0}^{\infty}q'_n(\rho,h)(\mu\cdot 1)^n, \qquad (47)$$

in which $q'_n(\rho,h)=h^n q_n(\rho,h)$ and $\mu\cdot 1=\tau/h=\mu t/h=\mu h/h=$the radius of the disk source measured in mean-free-paths of the attenuating medium, and $q'_0(\rho,h)=q_0(\rho,h)$.

For $h=0$, $\rho>1$ the expression in (37) reduces to

$$q_0(\rho,0)=\ln\left(\frac{\rho^2}{\rho^2-1}\right). \tag{48}$$

4. Buildup Factor

When both source and detector are embedded in a homogeneous medium, the secondary, or scattered radiation contribution I^s is often taken into account by means of a buildup factor [6]

$$B(\mu r)=(I^o+I^s)/I^o.$$

Such a buildup factor may then be used to evaluate the total flux I from a point isotropic source according to

$$I=I^o+I^s=I^oB(\mu r)=(\sigma/4\pi)B(\mu r)\exp(-\mu r)/r^2. \tag{49}$$

In references [8] and [9] $B(\mu r)$ is expressed as a set of polynomial coefficients β_i, in the notation of reference [9], as defined in equation (2), with $N=3$.

Now, since the integration of (33) was performed term by term over the expansion

$$\exp(-\tau/\cos\theta)=\exp(-\mu r)=\sum_{n=0}^{\infty}(-1)^n(\mu r)^n/n!, \tag{50}$$

no new integrands appear if these series terms are multiplied by terms $\beta_i(\mu r)^i$ of the polynomial representation of $B(\mu r)$. If this multiplication is performed, the total radiation flux as defined in (49) may be written as the series

$$I=I^o+I^s=(\sigma/4\pi)\sum_{n=0}^{\infty}\beta'_n\, q_n\tau^n, \tag{51}$$

in which $\tau=\mu h$. The modified buildup coefficients β'_n are generated from β_i's, such as are given in [8] or [9], as

$$\beta'_n=\sum_{i=0}^{N}(-1)^i\{n!/(n-i)!\}\beta_i \tag{52}$$

in which $n!/(n-i)!=0$ for $i>n$. For $N=3$ the

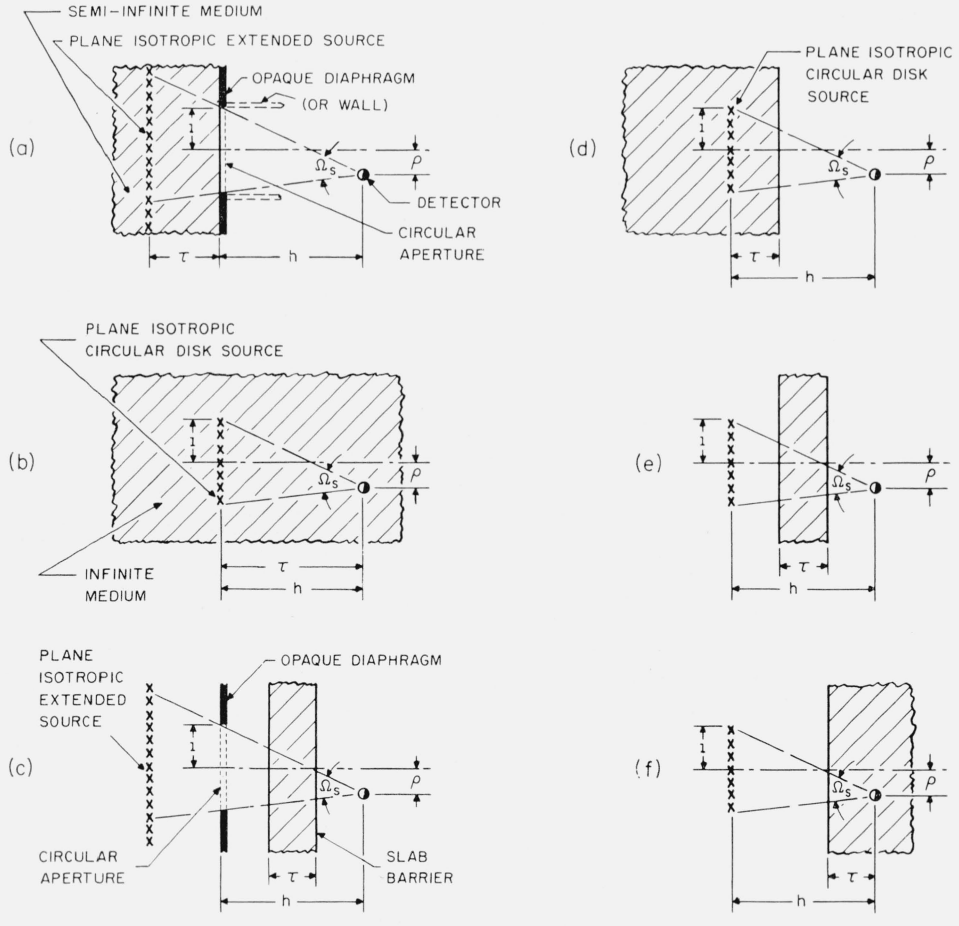

FIGURE 5. *Some circular aperture or disk source situations to which results are applicable. (a): I^o+I^s calculable using $p_l(p,h)$, $q_l(\tau)$ coefficients. (b): I^o+I^s calculable using β'_l,$q_l(\rho,h)$ coefficients. (a–f): I^o calculable using either $p_l(\rho,h)$ and $g_l{}^o$, or $q_l(\rho,h)$ coefficients.*

first five modified buildup coefficients are

$$\left.\begin{aligned}
&\beta_0'=\beta_0\simeq 1\\
&\beta_1'=\beta_0-\beta_1\\
&\beta_2'=\beta_0-2\beta_1+2\cdot 1\beta_2\\
&\beta_3'=\beta_0-3\beta_1+3\cdot 2\beta_2-3\cdot 2\cdot 1\beta_3\\
&\text{and}\\
&\beta_4'=\beta_0-4\beta_1+4\cdot 3\beta_2-4\cdot 3\cdot 2\beta_3.
\end{aligned}\right\} \quad (53)$$

Such a set of β_n' coefficients, once generated, may be applied as in (51) to either the disk-source $q_n(\rho,h)$'s in table 3 of this work or the rectangular source $q_n(a,b)$'s in table 3 of reference [3].

5. Discussion

Situations to which results in this paper may be applied are schematized in figure 5.

The Legendre method of section 2 can be used to calculate $I=I^o+I^s$ in such cases as figure 5a in which the source is distributed in a uniform layer (or layers) parallel to the exit surface of the medium. If g_l angular harmonic coefficients are used which have been calculated assuming an infinite medium, the result will be an overestimate because of the depression, in the realistic case, of flux near a boundary. This flux depression results from the one-way nature of the radiation traversal across the boundary. For gamma rays the infinite medium g_l's may be a rather good approximation, whereas for neutrons more realistic g_l's including the boundary effect may have to be used.

The unscattered component I^o may in principle be calculated for all situations in figure 5a–f using either the Legendre $p_l(\rho,h)$'s of section 2 or the $q_n(\rho,h)$'s of section 3, but in practice the Legendre series (6) converges better for barriers of the order of one mean free path or thicker while the $q_n(\rho,h)$ series (34) converges better for barriers of less than a mean free path.

Adaptation of polynomial representations of point isotropic source buildup factors, as suggested in section 4 for use with the $q_n(\rho,h)$'s of section 3 for computation of $I=I^o+I^s$, is strictly valid only for the situation in figure 5b, although some qualitative results may be obtained in the other situations depending on how little the physical situation departs from figure 5b.

The authors thank M. J. Berger and L. V. Spencer for their interest, encouragement and helpful criticisms regarding this effort. The authors are also indebted to A. B. Chilton, E. W. Emery, D. C. Kleinecke, J. H. Smith, and M. L. Storm for their reviews of the manuscript and suggestions towards clarity and accuracy of presentation.

6. References

[1] For an excellent review of this literature, see A. I. Mahan and W. F. Malmborg, Radiation characteristics of semicircular, circular and rectangular surface sources, J. Opt. Soc. Am. **44,** 644 (1954).

[2] J. H. Smith and M. L. Storm, Generalized off-axis distributions from disk sources of radiation, J. Appl. Phys. **25,** 519 (1954).

[3] J. H. Hubbell, R. L. Bach, and J. C. Lamkin, Radiation field from a rectangular source, J. Research NBS **64C,** 121 (1960).

[4] M. J. Berger and J. C. Lamkin, Sample calculations of gamma-ray penetration into shelters: Contributions of sky shine and roof contamination, J. Research NBS **60,** 109 (1958) RP2827.

[5] L. V. Spencer, Structure shielding against fallout radiation from nuclear weapons (to be published as an NBS Monograph).

[6] U. Fano. L. V. Spencer, and M. J. Berger, Penetration and diffusion of X-rays, Encyclopedia of physics (Springer-Verlag **38** II, 1959).

[7] I. G. Weinberg and E. R. Cohen, Neutron-flux distribution from a thermal column face, Nucleonics **13,** No. 7, 25 (1955).

[8] J. H. Hubbell, Dose due to distributed gamma-ray sources (unpublished).

[9] M. A. Capo, Polynomial approximation of gamma ray buildup factors for a point isotropic source, APEX–510, Nov. 1958.

[10] A. H. Jaffey, Solid angle subtended by a circular aperture at point and spread sources: Formulas and some tables, Rev. Sci. Instr. **25,** 349 (1954).

[11] A. V. H. Masket, R. L. Macklin, and H. W. Schmitt, Tables of solid angles and activations, ORNL–2170 (Nov. 1956).

[12] L. F. Epstein and J. H. Hubbell, Evaluation of a generalized elliptic-type integral (to be published).

[13] A. Fletcher, Guide to tables of elliptic functions, Mathematical tables and other aids to computation, **3,** 229 (1948–49).

[14] C. Hastings, Jr., Approximations for digital computers (Princeton Univ. Press, 1955).

[15] W. Gröbner and N. Hofreiter, Integraltafel II, Bestimmte Integrale (Springer-Verlag, 1958); see esp. eq 332.38a.

[16] Although identifiable with a result of R. A. Herman, A treatise on geometrical optics (Cambridge Univ. Press, London, 1900), p. 217, ex. 13, the form of the result in (29) seems to have first been published by P. D. Foote, Bull. NBS **12,** 583 (1915).

[17] G. Placzek, The functions $E_n(x)=\int_1^\infty e^{-xu}u^{-n}du$, MT–1, NRC No. 1547, Chalk River, Ont. (1946).

[18] R. M. Sievert, Die Intensitätsverteilung der primären γ-Strahlung in der Nähe medizinischer Radiumpräparate, Acta Radiol. (Stockholm) **1,** 89 (1921).

[19] See, for example, H. B. Dwight, Tables of integrals and other mathematical data, 3d ed., p. 2, eq 5.3–5.5 (McGraw-Hill, N.Y., 1957).

[20] See, for example, Nuclear engineering handbook, H. Etherington, ed.: Ch. 7.3, Nuclear radiation shielding, E. P. Blizard, p. 7–104 (McGraw-Hill, N.Y., 1958).

[21] E. Fermi, Sul moto dei neutroni nelle sostanze idrogenate, Ricerca Sci. **7,** part 2, 13 (1936)

[22] G. Placzek, The angular distribution of neutrons emerging from a plane surface, Phys. Rev. **72,** 556 (1947).

(Paper 65C4–78)